

# Effects of Nonmagnetic Impurities and Subgap States on the Kinetic Inductance, Complex Conductivity, Quality Factor, and Depairing Current Density

Takayuki Kubo<sup>1,2,\*</sup>

<sup>1</sup>High Energy Accelerator Research Organization (KEK), Tsukuba, Ibaraki 305-0801, Japan

<sup>2</sup>The Graduate University for Advanced Studies (Sokendai), Hayama, Kanagawa 240-0193, Japan



(Received 6 October 2021; revised 18 December 2021; accepted 24 December 2021; published 14 January 2022)

We investigate how a combination of a nonmagnetic impurity scattering rate  $\gamma$  and finite subgap states parametrized by Dynes  $\Gamma$  affects various physical quantities relevant to superconducting devices made from extreme type-II  $s$ -wave superconductors. All the calculations are based on the Eilenberger formalism of the BCS theory. It is well known that the optimum impurity concentration minimizes the surface resistance  $R_s$ . We find the optimum  $\Gamma$  can also reduce  $R_s$  by one order of magnitude for a clean superconductor ( $\gamma/\Delta_0 < 1$ ) and a few tens of % for a dirty superconductor ( $\gamma/\Delta_0 > 1$ ). Here,  $\Delta_0$  is the pair potential for the idealized ( $\Gamma \rightarrow 0$ ) BCS superconductor for  $T \rightarrow 0$ . Also, we find a nearly ideal ( $\Gamma/\Delta_0 \ll 1$ ) clean-limit superconductor exhibits a frequency-independent  $R_s$  for a broad range of frequency  $\omega$ , which can significantly improve  $Q$  of a compact cavity with a few tens of GHz frequency. As  $\Gamma$  or  $\gamma$  increases,  $R_s$  obeys the  $\omega^2$  dependence. The subgap-state-induced residual surface resistance  $R_{\text{res}}$  is also studied, which can be detected by a high- $Q$  three-dimensional resonator. We calculate the kinetic inductance  $L_k(\gamma, \Gamma, T)$  and the depairing current density  $J_d(\gamma, \Gamma, T)$ , which are monotonic increasing and decreasing functions of  $(\gamma, \Gamma, T)$ , respectively. Measurements of  $(\gamma, \Gamma)$  of device materials can give helpful information on improving  $Q$ , engineering  $L_k$ , and ameliorating  $J_d$  via materials processing.

DOI: [10.1103/PhysRevApplied.17.014018](https://doi.org/10.1103/PhysRevApplied.17.014018)

## I. INTRODUCTION

The microscopic theory of superconductivity is the linchpin of research and development of various superconducting devices, such as superconducting radio-frequency (SRF) cavities for particle accelerators [1–3], superconducting magnets and cables [4], kinetic inductance detectors (KIDs) [5], hot-electron bolometer [6], other superconducting instruments for astrophysics and cosmology [7], superconducting single-photon detectors (SSPDs) [8,9], and superconducting qubits for quantum-information processing (QIP) [10,11]. Models of superconducting devices based on the idealized BCS superconductor without any pair breakers usually provide good starting points to understand the operating principles of these technologies. However, such models are sometimes too naive to analyze the physics of real devices. The representative example is the quality factor  $Q$  of superconducting resonators. The surface resistance and then  $Q$  are sensitive to the detail of the quasiparticle density of states (DOSSs), which is affected by various pair breakers in the real world, such as the current and magnetic impurities [12–16]. Hence, an analysis of  $Q$  based on the ideal

BCS DOS, i.e., the Mattis-Bardeen (MB) theory [17], is qualitative and sometimes inadequate even for qualitative analyses. In fact, the MB theory cannot explain the rf-field-dependent nonlinear  $Q$ , effects of material treatment on  $Q$ , and saturation of  $Q$  at  $T \rightarrow 0$ . Another example is the depairing current density  $J_d$ . The well-known Kupriyanov-Lukichev-Maki theory [18,19] gives  $J_d$  for the ideal BCS superconductor. However, pair breakers in device materials (e.g., magnetic impurities) can degrade  $J_d$  and thus reduce the ultimate limit of the current density in superconducting cables and that of the accelerating field of the SRF cavity [20]. To understand the physics of superconducting devices and to discern the causes of unexpected performance limitations of real devices, we need to take various pair breakers in real materials into account (e.g., current, magnetic impurities, metallic suboxides, hydride, and nonstoichiometric regions) and to assess the effects of such nonideal features on device performances [21,22].

One of the nonideal features observed in various superconducting materials is the broadening and subgap states in DOS [23–33], in contrast to the sharp spectrum gap in the idealized BCS superconductor. Various mechanisms can contribute to the subgap states, e.g., inelastic scattering of quasiparticles on phonons [34,35], Coulomb correlations [36], anisotropy of the Fermi surface [37], local inhomogeneities of the BCS pairing constant [38],

\*kubotaka@post.kek.jp; stay-at-home dad on two-year paternity leave, New York, NY, USA.

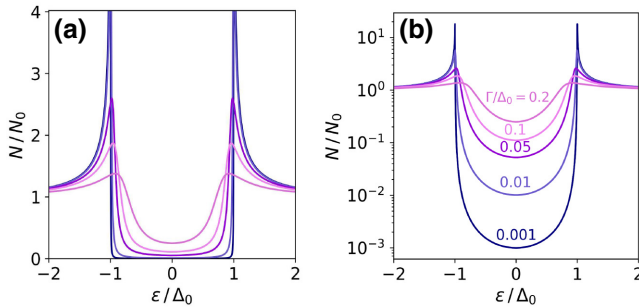


FIG. 1. (a) Quasiparticle DOSs at  $T \rightarrow 0$  calculated for  $\Gamma/\Delta_0 = 0.2, 0.1, 0.05, 0.01$ , and  $0.001$ . (b) DOS in a logarithmic scale. Note the DOS in the zero-current state is independent of a concentration of nonmagnetic impurities.

magnetic impurities [39], and effects of spatial correlations in impurity scattering [40]. Such a broadened DOS is often described by using the phenomenological Dynes formula [41,42] (see also Fig. 1),

$$\frac{N(\epsilon)}{N_0} = \text{Re} \frac{\epsilon + i\Gamma}{\sqrt{(\epsilon + i\Gamma)^2 - \Delta^2}}. \quad (1)$$

Here  $\Delta$  is the pair potential,  $N_0$  is the normal-state DOS at the Fermi level, and  $\Gamma$  is the Dynes broadening parameter. We can reproduce the ideal BCS DOS by taking  $\Gamma \rightarrow 0$ . Irrespective of microscopic models of the Dynes formula, we can incorporate  $\Gamma$  into the quasiclassical formalism of the BCS theory (see, e.g., Refs. [21,22,43–46]). The microscopic derivation of Eq. (1) is still an open question, while some models have been investigated [47,48].

The first way to calculate physical quantities based on a realistic spectrum is to incorporate all the broadening mechanisms in materials into a device model. However, such a model should contain a bunch of free parameters, which is practically useless unless those parameters are determined from a number of experiments. Another way is to introduce the phenomenological Dynes  $\Gamma$  into a device model. Here, a value of  $\Gamma$  can be determined from experiments such as tunneling spectroscopy [23], angle-integrated photoemission spectroscopy (AIPES) [32], and measurements of complex conductivity [49,50]. Even if we do not know what kind of pair breakers contribute to subgap states, such an experimentally determined  $\Gamma$  makes it possible to calculate physical quantities based on the realistic quasiparticle spectrum. In the present paper, we pursue the second approach, which would give reliable results rather than those based on the idealized BCS DOS.

According to the previous studies for the diffusive limit [21,22,43,44], influences of a finite  $\Gamma$  are far reaching: it affects, e.g., the pair potential  $\Delta$ , the critical temperature  $T_c$ , the penetration depth  $\lambda$ , the kinetic inductivity  $L_k$ , the complex conductivity  $\sigma$ , the coherence peak of dissipative conductivity  $\sigma_1$ , the surface impedance,  $Q$  factor, and the

depairing current density  $J_d$ . One of the nontrivial consequences is the fact that there exists the optimum  $\Gamma$ , which maximizes  $Q$  at some temperature range [3,21,22,43]. This  $\Gamma$ -induced  $Q$  rise comes from the same mechanism as the  $Q$  rise due to current-induced DOS broadening [51,52]. On the other hand, finite subgap states in the vicinity of the Fermi level induce a residual dissipative conductivity,  $\lim_{T \rightarrow 0} \sigma_1$  [2,3,21,43,53].

The effects of a finite  $\Gamma$  in a moderately clean superconductor have been studied less extensively except for some calculations of  $\sigma$  [49,53]. In the present study, we investigate the effects of a combination of Dynes  $\Gamma$  and nonmagnetic impurity scattering rate  $\gamma$  on the kinetic inductivity  $L_k$ , the surface resistance  $R_s$ , and the depairing current density  $J_d$ , which are the physical quantities relevant to modern superconducting devices. The kinetic inductance is known to limit the reset time after a detection event of SSPDs [54] and also plays an essential role in the operating mechanism of KIDs, which detects a shift of resonant frequency  $\delta f \propto -\delta L_k$  due to the arrival of pair-breaking photons [5]. The surface resistance  $R_s$  is proportional to the dissipation at the inner surface of a three-dimensional (3D) resonant cavity for SRF and QIP. Reduction of  $R_s$  (or improvement of  $Q$ ) has been the primary interest of researchers of resonant cavities over the last decades. Vortex-free Nb cavities [55–60] exhibit a huge quality factor  $Q \sim 10^{10}\text{--}10^{12}$  at  $T < 2$  K [61–64] even under the strong rf current [65–68] close to the depairing current density. The depairing current density  $J_d$  is related to the bias current of SSPD and is the maximum current that SRF cavities and superconducting cables can support. The screening current density on the inner surface of the cutting-edge Nb cavity reaches a current density close to  $J_d$ , and SRF researchers study next-generation cavities using alternative materials with higher  $J_d$  theoretically [69–74] and experimentally [75–85].

Our calculations are based on the well-established Eilenberger formalism of the BCS theory [16,86], which can include an arbitrary impurity concentration. We assume that the penetration depth  $\lambda$  is much larger than the coherence length  $\xi$ , then a superconductor obeys the local electrodynamics. Large- $\lambda/\xi$  superconductors include dirty Nb and also NbN, Nb-Ti-N, and Nb<sub>3</sub>Sn for any impurity concentration from the clean limit to the dirty limit.

The paper is organized as follows. In Sec. II, we briefly review the Eilenberger formalism of the BCS theory [16,86] and basic consequences of a finite  $\Gamma$  in the zero-current state. In Sec. III, we evaluate the penetration depth  $\lambda(\gamma, \Gamma, T)$  and the kinetic inductivity  $L_k(\gamma, \Gamma, T)$ . Convenient formulas for  $\lambda$  and  $L_k$  are also summarized. In Sec. IV, we summarize the complex conductivity formulas, evaluate the  $T$  dependence and the coherence peak, and consider the low  $T$  limit and moderately low  $T$  regime ( $\hbar\omega \ll k_B T \ll \Delta_0$ ). Then, combining the results of Secs. III and IV A–IV D, we study the effects of  $(\gamma, \Gamma)$

on the surface resistance and  $Q$  factor in the low  $T$  limit and the moderately low  $T$  regime. In Sec. V, we solve the Eilenberger equation in the current-carrying state and evaluate the effects of  $(\gamma, \Gamma)$  on the depairing current density  $J_d$ . In Sec. VI, we discuss the implications of our results.

## II. THEORY

### A. Eilenberger equation

The normal ( $g_m$ ) and anomalous ( $f_m$ ) quasiclassical Matsubara Green's functions obey the Eilenberger equation [16,86]. Since we consider the case  $\lambda \gg \xi$ , the current distribution varies slowly over the coherence length, and then the spatial-differentiation terms are negligible. The Eilenberger equation for the current-carrying state reduces to

$$\left[ i \frac{\pi s}{2} \cos \theta + (\hbar \omega_m + \Gamma) \right] f_m - \Delta g_m = \gamma \{ \langle f_m \rangle g_m - \langle g_m \rangle f_m \}. \quad (2)$$

Here,  $g_m^2 + f_m^2 = 1$ ,  $\hbar \omega_m = 2\pi k_B T(m + 1/2)$  is the Matsubara frequency,  $\Gamma$  is the Dynes parameter,  $\gamma = \hbar/2\tau_{\text{imp}}$  is the nonmagnetic impurity scattering rate,  $\tau_{\text{imp}}$  is the electron scattering time on nonmagnetic impurities,  $s = \hbar q v_f / \pi = (q/q_0) \Delta_0$ ,  $\hbar q$  is the superfluid momentum,  $v_f$  is the Fermi velocity,  $q_0 = 1/\xi_0 = \pi \Delta_0 / \hbar v_f$  is the inverse of the BCS coherence length,  $\Delta$  is the pair potential,  $\Delta_0$  is the pair potential of the idealized ( $\Gamma \rightarrow 0$ ) BCS superconductor in the zero-current state ( $q = 0$ ) at  $T \rightarrow 0$ ,  $\theta$  is the angle between the Fermi velocity and the current, and the bracket  $\langle X \rangle$  is the angular averaging of a quantity  $X$  over the Fermi surface. We assume a spherical Fermi surface:  $\langle X \rangle = (1/2) \int_0^\pi X \sin \theta d\theta$ . Note here that considering the average distance the electron travels between electron-nonmagnetic impurity collisions is given by  $\ell_{\text{imp}} = v_f \tau_{\text{imp}}$ , we obtain the relation  $\ell_{\text{imp}}/\xi_0 = \pi \Delta_0 / 2\gamma$ .

In the zero-current state ( $q = 0$ ), the  $\theta$  dependences of  $f_m$  and  $g_m$  drop off:  $\langle f_m \rangle = f_m$  and  $\langle g_m \rangle = g_m$ . Then, Eq. (2) reduces to

$$(\hbar \omega_m + \Gamma) f_m - \Delta g_m = 0, \quad (3)$$

which no longer includes the nonmagnetic impurity scattering rate  $\gamma$ . Hence, in the zero-current state,  $\Delta$  does not depend on a concentration of nonmagnetic impurities. This robustness of  $s$ -wave superconductor to nonmagnetic impurity is known as Anderson's theorem [16].

The Eilenberger equation is compensated by the self-consistency equation

$$\ln \frac{T_{c0}}{T} = 2\pi k_B T \sum_{\omega_m > 0} \left( \frac{1}{\hbar \omega_m} - \frac{\langle f_m \rangle}{\Delta} \right). \quad (4)$$

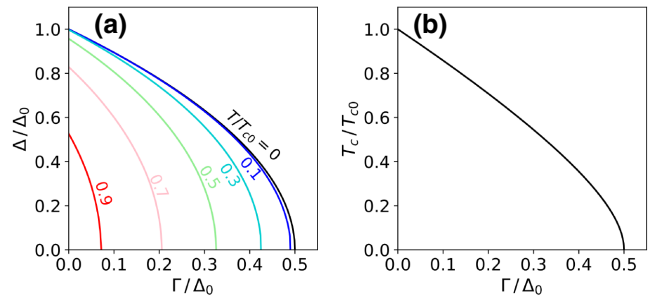


FIG. 2. (a) Pair potential  $\Delta$  as functions of  $\Gamma$ , calculated for  $T/T_{c0} = 0, 0.1, 0.3, 0.5, 0.7$ , and  $0.9$ . (b) Critical temperature  $T_c$  as a function of  $\Gamma$ .

Here,  $k_B T_{c0} = \Delta_0 \exp(\gamma_E)/\pi \simeq \Delta_0/1.76$  is the critical temperature of the idealized ( $\Gamma \rightarrow 0$ ) BCS superconductor, and  $\gamma_E = 0.577$  is Euler's constant. Solving Eqs. (2) and (4) for the current-carrying state or Eqs. (3) and (4) for the zero-current state, we can calculate various physical quantities.

### B. Brief review of the consequences of a finite $\Gamma$ in the zero-current state

Let us briefly review the effects of finite Dynes subgap states on  $\Delta$ ,  $T_c$ , and DOS in the zero-current state. This short review provides the basic knowledge necessary for the discussions in the following sections.

Solving Eq. (3), we get

$$g_m = \frac{\hbar \omega_m + \Gamma}{\sqrt{(\hbar \omega_m + \Gamma)^2 + \Delta^2}}, \quad (5)$$

$$f_m = \frac{\Delta}{\sqrt{(\hbar \omega_m + \Gamma)^2 + \Delta^2}}. \quad (6)$$

Here,  $\Delta = \Delta(\Gamma, T)$  is calculated from Eq. (4). For  $T \rightarrow 0$ , it is easy to find [21,22,43,44,48,49,53]

$$\Delta(\Gamma, T)|_{T \rightarrow 0} = \Delta_0 \sqrt{1 - 2 \frac{\Gamma}{\Delta_0}}. \quad (7)$$

Hence, the zero-temperature pair potential vanishes at the critical value  $\Gamma = \Delta_0/2$ . Equation (7) reduces to  $\simeq \Delta_0 - \Gamma$  when  $\Gamma/\Delta_0 \ll 1$ . A calculation for an arbitrary temperature is straightforward. Shown in Fig. 2(a) is  $\Delta$  as functions of  $\Gamma$  for different temperatures. The larger the temperature is, the smaller the critical value is.

The critical temperature  $T_c = T_c(\Gamma)$  is obtained by substituting  $T \rightarrow T_c$  and  $\Delta \rightarrow 0$  into Eq. (4). We find [21,22,43,44,48]

$$\ln \frac{T_c}{T_{c0}} = \psi\left(\frac{1}{2}\right) - \psi\left(\frac{1}{2} + \frac{\Gamma}{2\pi k_B T_c}\right). \quad (8)$$

Here,  $\psi$  is the digamma function. Equation (8) reduces to  $T_c \simeq T_{c0} - \pi \Gamma / 4k_B$  for  $\Gamma/\Delta_0 \ll 1$ . It should be noted

that Eq. (8) has the same form as the well-known formula of critical temperature for a superconductor with pair-breaking perturbations [12–16]. Shown in Fig. 2(b) is  $T_c$  as a function of  $\Gamma$ , which is a monotonically decreasing function of  $\Gamma$  and vanishes at  $\Gamma = \Delta_0/2$ .

In the real frequency representation ( $\hbar\omega_m \rightarrow -i\epsilon$ ), we get

$$g(\epsilon) = \frac{\epsilon + i\Gamma}{\sqrt{(\epsilon + i\Gamma)^2 - \Delta^2}}, \quad (9)$$

$$f(\epsilon) = \frac{\Delta}{\sqrt{(\epsilon + i\Gamma)^2 - \Delta^2}}. \quad (10)$$

The quasiparticle DOS is given by  $N(\epsilon)/N_0 = \text{Re}[g]$ , which corresponds with the Dynes formula shown in Sec. I [see Eq. (1) and Fig. 1].

The Dynes  $\Gamma$  is a phenomenological representation of some pair breakers in real materials. Introducing  $\Gamma$  not only yields the broadened DOS (see Fig. 1) but also results in various pair-breaking effects (e.g., suppression of  $\Delta$  and  $T_c$  shown in Fig. 2). In the zero-current state,  $\Delta$ ,  $T_c$ , and DOS are independent of a concentration of nonmagnetic impurities (Anderson theorem). Hence, the results shown in Sec. II B are coincident with those for the dirty limit discussed in the previous studies [21,22,43,44]. In the following sections, we study physical quantities that depend on the Dynes  $\Gamma$  and the nonmagnetic impurity scattering rate  $\gamma$ .

### III. PENETRATION DEPTH AND KINETIC INDUCTANCE

#### A. Penetration depth

First, consider the penetration depth in the zero-current limit. The penetration depth  $\lambda(\gamma, \Gamma, T)$  is calculated from [16]

$$\frac{1}{\lambda^2(\gamma, \Gamma, T)} = \frac{2\pi k_B T}{\lambda_0^2} \sum_{\omega_m > 0} \frac{f_m^2}{d_m}. \quad (11)$$

Here,  $\lambda_0^{-2} = \lambda^{-2}(0, 0, 0) = (2/3)\mu_0 e^2 N_0 v_f^2 = \mu_0 e^2 n/m$  is the idealized BCS penetration depth in the clean limit at  $T \rightarrow 0$ ,  $f_m$  is given by Eq. (6), and  $d_m = \sqrt{(\hbar\omega_m + \Gamma)^2 + \Delta^2} + \gamma$ . Analytical expressions of  $\lambda$  can be obtained for some special cases, e.g., a nearly ideal ( $\Gamma/\Delta_0 \ll 1$ ) moderately clean ( $\gamma/\Delta_0 \ll 1$ ) superconductor at  $T \rightarrow 0$ . The summation can be replaced with integral ( $2\pi k_B T/\hbar \sum_{\omega_m > 0} \rightarrow \int_0^\infty d\omega$ ) when  $T \rightarrow 0$ , and we find

$$\frac{1}{\lambda^2(\gamma \ll \Delta_0, \Gamma \ll \Delta_0, 0)} = \frac{1}{\lambda_0^2} \left( 1 - \frac{\Gamma}{\Delta_0} - \frac{\pi\gamma}{4\Delta_0} \right). \quad (12)$$

Another example is the idealized ( $\Gamma \rightarrow 0$ ) BCS superconductor at  $T \rightarrow 0$  including an arbitrary concentration

of nonmagnetic impurities. Replacing the summation with integral, Eq. (11) reduces to the well-known formula (see, e.g., Ref. [2,3,87]):

$$\begin{aligned} & \frac{1}{\lambda^2(\gamma, 0, 0)} \\ &= \begin{cases} \frac{1}{\lambda_0^2 \gamma / \Delta_0} \left( \frac{\pi}{2} - \frac{\cos^{-1}(\gamma/\Delta_0)}{\sqrt{1 - (\gamma/\Delta_0)^2}} \right) & (\gamma/\Delta_0 < 1) \\ \frac{1}{\lambda_0^2} \left( \frac{\pi}{2} - 1 \right) & (\gamma/\Delta_0 = 1) \\ \frac{1}{\lambda_0^2 \gamma / \Delta_0} \left( \frac{\pi}{2} - \frac{\cosh^{-1}(\gamma/\Delta_0)}{\sqrt{(\gamma/\Delta_0)^2 - 1}} \right) & (\gamma/\Delta_0 > 1) \end{cases} \quad (13) \end{aligned}$$

In the dirty limit ( $\gamma/\Delta_0 = \pi\xi_0/2\ell_{\text{imp}} \gg 1$ ), substituting  $d_m \simeq \gamma$  into Eq. (11), we reproduce the formula derived in the previous study [21]:

$$\begin{aligned} & \frac{1}{\lambda^2(\gamma \gg \Delta_0, \Gamma, T)} \\ &= \frac{4k_B T}{\lambda_{0,\text{dirty}}^2 \Delta_0} \sum_{\omega_m > 0} f_m^2 \\ &= \frac{2\Delta(\Gamma, T)}{\lambda_{0,\text{dirty}}^2 \pi \Delta_0} \text{Im}\psi\left(\frac{1}{2} + \frac{\Gamma}{2\pi k_B T} + i\frac{\Delta(\Gamma, T)}{2\pi k_B T}\right). \quad (14) \end{aligned}$$

Here,  $\lambda_{0,\text{dirty}}^{-2} = (\pi\Delta_0/2\gamma)\lambda_0^{-2} = \pi\mu_0\Delta_0\sigma_n/\hbar$  is the well-known BCS penetration depth in the dirty limit at  $T \rightarrow 0$ , and  $\psi$  is the digamma function. For the idealized dirty-limit BCS superconductor, Eq. (14) simplifies to [12,16]

$$\frac{1}{\lambda^2(\gamma \gg \Delta_0, 0, T)} = \frac{\Delta(0, T)}{\lambda_{0,\text{dirty}}^2 \Delta_0} \tanh \frac{\Delta(0, T)}{2k_B T}. \quad (15)$$

Equation (15) is widely used when analyzing experimental data of superconducting devices, but its range of applicability is somewhat limited.

To evaluate  $\lambda$  for an arbitrary  $(\gamma, \Gamma, T)$ , we need to calculate Eq. (11) numerically. Shown in Fig. 3 is  $\lambda$  as functions of (a)  $\gamma$  and (b)  $\Gamma$  for different temperatures:  $\lambda$  is a monotonic increasing function of  $\gamma$ ,  $\Gamma$ , and  $T$ . The rapid increases of  $\lambda$  at  $\Gamma/\Delta_0 \gtrsim 0.1$  come from the pair-breaking effect of  $\Gamma$  close to its critical value (see also Fig. 2 and Ref. [44]).

#### B. Kinetic inductance

The direct application of the results of Sec. III A is calculations of the kinetic inductance in the zero-current state, which is a crucial physical quantity for superconducting devices, such as KIDs and SSPDs. The kinetic inductance of a thin and narrow film is given by  $L_{\text{film}} = [\text{length}/(\text{width} \times \text{thickness})] \times L_k$ . Here,  $L_k$  is the kinetic

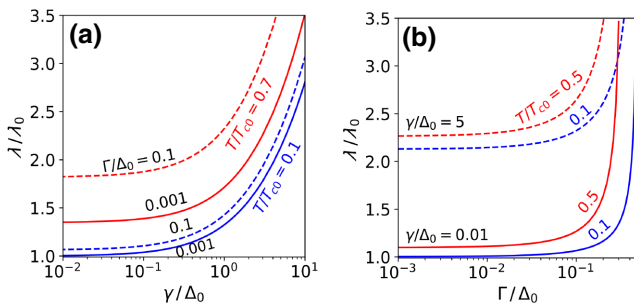


FIG. 3. Penetration depth  $\lambda(\gamma, \Gamma, T)$  as functions of (a) nonmagnetic impurity scattering rate  $\gamma/\Delta_0 = \pi\xi_0/2\ell_{\text{imp}}$  and (b) Dynes parameter  $\Gamma$ .

inductivity. In the zero-current limit,  $L_k$  is given by  $L_k = \mu_0\lambda^2$  (see also Refs. [44,88,89] for  $L_k$  of a dirty-limit superconductor under the current). Since we already calculate  $\lambda$  in Sec. III A, we have almost finished the calculations of  $L_k$ ; see Fig. 4.

For readers' convenience, let us summarize the analytical formulas of  $L_k$  in the zero-current limit ( $q \rightarrow 0$ ). For a superconductor including an arbitrary impurity concentration,  $L_k$  is given by

$$L_k(\gamma, \Gamma, T) = L_{k0} \frac{\lambda^2(\gamma, \Gamma, T)}{\lambda_0^2}. \quad (16)$$

Here,  $L_{k0} = L_k(0, 0, 0) = \mu_0\lambda_0^2 = 3/2e^2N_0v_f^2$  is the kinetic inductivity for an idealized ( $\Gamma \rightarrow 0$ ) clean-limit ( $\gamma \propto \ell_{\text{imp}}^{-1} \rightarrow 0$ ) BCS superconductor at  $T \rightarrow 0$ . In the dirty limit ( $\gamma/\Delta_0 = \pi\xi_0/2\ell_{\text{imp}} \gg 1$ ), taking  $d_m \rightarrow \gamma$ , we get

$$L_k(\gamma \gg \Delta_0, \Gamma, T) = L_{k0,\text{dirty}} \frac{\lambda^2(\gamma \gg \Delta_0, \Gamma, T)}{\lambda_{0,\text{dirty}}^2}. \quad (17)$$

Here,  $L_{k0,\text{dirty}} = \mu_0\lambda_{0,\text{dirty}}^2 = \hbar/\pi\Delta_0\sigma_n$  is the inductivity of the idealized ( $\Gamma \rightarrow 0$ ) dirty-limit BCS superconductor at  $T \rightarrow 0$ . Substituting Eqs. (12) or (13) into Eq. (16) or substituting Eqs. (14) or (15) into Eq. (17), we can analytically evaluate  $L_k$ .

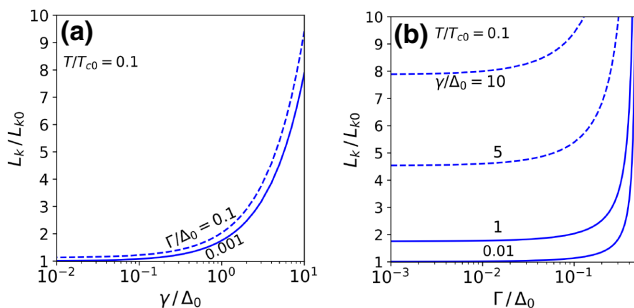


FIG. 4. Kinetic inductivity at  $T/T_{c0} = 0.1$  as functions of (a) nonmagnetic impurity scattering rate  $\gamma/\Delta_0 = \pi\xi_0/2\ell_{\text{imp}}$  and (b) Dynes  $\Gamma$  parameter.

It should be noted that, Eqs. (15) and (17) yield the widely used formula,  $L_k = [\hbar\rho_n/\pi\Delta(0, T)]/\tanh[\Delta(0, T)/2k_B T]$ , but it can apply only to the idealized ( $\Gamma \rightarrow 0$ ) dirty-limit ( $\gamma/\Delta_0 = \pi\xi_0/2\ell_{\text{imp}} \gg 1$ ) BCS superconductor. The other formulas introduced in this section are more general and would be available for various situations.

#### IV. COMPLEX CONDUCTIVITY, SURFACE IMPEDANCE, AND Q FACTOR

The complex conductivity and the surface impedance depend on the quasiparticle spectrum and the quasiparticle distribution function [51,90,91]. Under the microwave field, the screening current modifies the quasiparticle spectrum [12–16]. In addition, the quasiparticle distribution is not necessarily well described by the Fermi-Dirac function  $f_{\text{FD}} = [1 - \tanh(\epsilon/2k_B T)]/2$  [12,16]. Deviation depends on an absorbed microwave power and a rate of the energy transfer from quasiparticles to phonon. The previous study [22] calculated the distribution function under the microwave field using the Keldysh technique of the nonequilibrium Green's function and evaluated the nonequilibrium effect. Taking a Nb resonator, for example, the parameter  $(\Gamma/\Delta_0, T, \omega/2\pi, H_0/H_c) = (0.1, 2 \text{ K}, 1 \text{ GHz}, 0.5)$  is on the fuzzy boundary where the nonequilibrium effect becomes significant. Here,  $H_0$  is the amplitude of the microwave magnetic field, and  $H_c$  is the thermodynamic critical field. The nonequilibrium effect is diminished as  $\Gamma$  increases,  $T$  increases,  $\omega$  decreases, or  $H_0$  decreases. In the weak-field limit ( $H_0 \rightarrow 0$ ), the problem is significantly simplified: we may neglect the nonequilibrium effect and may use  $f_{\text{FD}}$  for the quasiparticle distribution function. The spectrum function is given by Eqs. (9) and (10). In this section, we focus on the weak-field limit and calculate the complex conductivity and the surface impedance using the well-established linear response formulas [17,87,92–95].

##### A. Complex-conductivity formulas

The general formula for the complex conductivity  $\sigma$  of a large- $\lambda/\xi$  superconductor, which can include an arbitrary concentration of nonmagnetic impurities, is given by [87,92–95]

$$\begin{aligned} \sigma(\gamma, \Gamma, T, \omega) &= \sigma_1 + i\sigma_2 \\ &= \frac{-i\sigma_n}{4\omega\tau} \int_{-\infty}^{\infty} d\epsilon \left[ I_1 \tanh \frac{\epsilon_-}{2kT} - I_2 \tanh \frac{\epsilon_+}{2kT} \right], \end{aligned} \quad (18)$$

$$I_1 = \frac{g_+g_- + f_+f_- - 1}{d_+ + d_-} + \frac{g_+g_-^* + f_+f_-^* + 1}{d_+ - d_-^*}, \quad (19)$$

$$I_2 = \frac{g_+^* g_-^* + f_+^* f_-^* - 1}{-d_+^* - d_-^*} + \frac{g_+ g_-^* + f_+ f_-^* + 1}{d_+ - d_-^*}. \quad (20)$$

Here,  $\sigma$  is a function of the impurity scattering rate  $\gamma/\Delta_0 = \pi\xi_0/2\ell_{\text{imp}}$ , the Dynes parameter  $\Gamma$ , temperature  $T$ , and the photon frequency  $\omega$ ;  $\sigma_n = (2/3)e^2 N_0 v_f^2 \tau$  is the dc conductivity in the normal state,  $\tau$  is the electron relaxation time,  $\epsilon_{\pm} = \epsilon \pm \hbar\omega/2$ ,  $g_{\pm} = g(\epsilon_{\pm})$ ,  $f_{\pm} = f(\epsilon_{\pm})$ ,  $d_{\pm} = d(\epsilon_{\pm})$ , and  $d(\epsilon) = \sqrt{(\epsilon + i\Gamma)^2 - \Delta^2 + i\gamma}$ .

In the normal state ( $\Delta \rightarrow 0$ ), we have  $g_{\pm} = 1$ ,  $f_{\pm} = 0$ , and  $d_+ - d_-^* = \hbar\omega + 2i(\Gamma + \gamma)$ . Then, Eq. (18) reduces to the Drude model of the ac electrical conductivity of normal metal:  $\sigma_{n1} = \sigma_n/[1 + (\omega\tau)^2]$  and  $\sigma_{n2} = \sigma_n\omega\tau/[1 + (\omega\tau)^2]$  with the electron relaxation time  $\tau$ ,

$$\frac{1}{\tau} = \frac{1}{\tau_{\text{imp}}} + \frac{1}{\tau_{\Gamma}}. \quad (21)$$

Here  $\tau_{\text{imp}} = \hbar/2\gamma$  and  $\tau_{\Gamma} = \hbar/2\Gamma$ . It is also possible to derive Eqs. (21) considering a microscopic origin of  $\Gamma$ : the electron-phonon scattering [94] and other models such as Ref. [48].

In the low-frequency regime ( $\hbar\omega \ll \gamma, \Gamma, k_B T, \Delta_0$ ), we can expand the integrand with respect to a tiny  $\omega$ . Then, Eq. (18) reduces to

$$\begin{aligned} \sigma_1(\gamma, \Gamma, T, 0) &= \frac{\sigma_n \hbar / \tau}{8k_B T} \int_{-\infty}^{\infty} d\epsilon \frac{1}{\cosh^2(\epsilon/2k_B T)} \\ &\times \left[ \frac{(\text{Re } g)^2}{\text{Im } d} + \frac{(\text{Re } d \text{ Im } f - \text{Im } d \text{ Re } f)^2}{\{(\text{Re } d)^2 + (\text{Im } d)^2\} \text{Im } d} \right], \end{aligned} \quad (22)$$

and

$$\begin{aligned} \sigma_2 &= \frac{\sigma_n}{2\tau\omega} \int_{-\infty}^{\infty} d\epsilon \tanh \frac{\epsilon}{2k_B T} \text{Re} \left[ \frac{f^2}{d} \right] \\ &= \frac{2e^2 N_0 v_f^2}{3\mu_0 \omega} 2\pi k_B T \sum_{\omega_m > 0} \frac{f_m^2}{d_m} = \frac{1}{\mu_0 \omega \lambda^2}, \end{aligned} \quad (23)$$

which are used in Ref. [49] to study the effects of  $\Gamma$  in the low-frequency regime.

In the dirty limit ( $\gamma/\Delta_0 = \pi\xi_0/2\ell_{\text{imp}} \gg 1$ ), we can take  $d_+ \simeq d_- \simeq i\gamma$ . Then, Eq. (18) reduces to the well-known formulas [92]:

$$\begin{aligned} \sigma_1(\gamma \gg \Delta_0, \Gamma, T, \omega) &= \frac{\sigma_n}{\hbar\omega} \int_{-\infty}^{\infty} d\epsilon [f_{\text{FD}}(\epsilon) - f_{\text{FD}}(\epsilon_{++})] M(\epsilon, \omega), \end{aligned} \quad (24)$$

$$M(\epsilon, \omega) = \text{Reg}(\epsilon)\text{Reg}(\epsilon_{++}) + \text{Ref}(\epsilon)\text{Ref}(\epsilon_{++}), \quad (25)$$

and

$$\sigma_2(\gamma \gg \Delta_0, \Gamma, T, \omega) = \frac{\sigma_n}{\hbar\omega} \int_{-\infty}^{\infty} d\epsilon \tanh \frac{\epsilon}{2k_B T} L(\epsilon, \omega), \quad (26)$$

$$L(\epsilon, \omega) = \text{Reg}(\epsilon)\text{Img}(\epsilon_{++}) + \text{Ref}(\epsilon)\text{Imf}(\epsilon_{++}). \quad (27)$$

Here,  $\epsilon_{++} = \epsilon + \hbar\omega$ . Equation (24) is used in Refs. [21,22,43] to study the impact of imperfect surfaces on  $Q$  factor. It should be noted that, for the idealized ( $\Gamma \rightarrow 0$ ) dirty-limit ( $\gamma/\Delta_0 \gg 1$ ) BCS superconductor, Eqs. (24) and (26) reproduce the textbook formulas [7,12]:

$$\begin{aligned} \sigma_1(\gamma \gg \Delta_0, \Gamma \rightarrow 0, T, \omega) &= \frac{2\sigma_n}{\hbar\omega} \int_{\Delta}^{\infty} d\epsilon \frac{[\epsilon(\epsilon + \hbar\omega) + \Delta^2][f_{\text{FD}}(\epsilon) - f_{\text{FD}}(\epsilon_{++})]}{\sqrt{\epsilon^2 - \Delta^2} \sqrt{\epsilon_{++}^2 - \Delta^2}}, \end{aligned} \quad (28)$$

and

$$\begin{aligned} \sigma_2(\gamma \gg \Delta_0, \Gamma \rightarrow 0, T, \omega) &= \frac{\sigma_n}{\hbar\omega} \int_{\Delta}^{\Delta+\hbar\omega} d\epsilon \tanh \frac{\epsilon}{2k_B T} \frac{\epsilon(\epsilon - \hbar\omega) + \Delta^2}{\sqrt{\epsilon^2 - \Delta^2} \sqrt{\Delta^2 - \epsilon_{--}^2}} \end{aligned} \quad (29)$$

for  $\hbar\omega < \Delta$ . Here,  $\epsilon_{--} = \epsilon - \hbar\omega$ .

Now, it would be evident that the famous handy formulas, Eqs. (28) and (29), can apply only to the special case and are usually not enough for quantitative understanding of dissipation in real devices, which generally include some pair breakers. The previous studies used Eqs. (24), (26) and their nonequilibrium version to investigate the effects of Dynes subgap states, strong rf current, magnetic impurities, and proximity-coupled normal layer at the surface [21,22,43,51]. In the following, we use Eq. (18), which can be applied to a superconductor with an arbitrary impurity concentration, to investigate how a combination of subgap states ( $\Gamma$ ) and nonmagnetic impurities ( $\gamma$ ) affects  $\sigma$  and  $Q$ .

## B. Temperature dependence of $\sigma_1$ and coherence peak

First, consider the effect of the Dynes  $\Gamma$  and the nonmagnetic impurity scattering rate  $\gamma \propto \xi_0/\ell_{\text{imp}}$  on the temperature dependence of  $\sigma_1$  and the coherence peak. See also the recent study [49], in which they studied  $\sigma_1(T)$  for  $\omega \rightarrow 0$ .

To examine  $\sigma_1(T)$ , we need the temperature dependence of  $\Gamma$ . Some materials exhibit nearly constant  $\Gamma$  for  $T/T_c \lesssim 0.5$  (e.g., MoC [29], Nb [32], Pb [32]), while some do not [31]. Also, the microscopic origin of Eq. (1) is still an open question, and theoretical  $\Gamma(T)$  is unclear. Hence, in

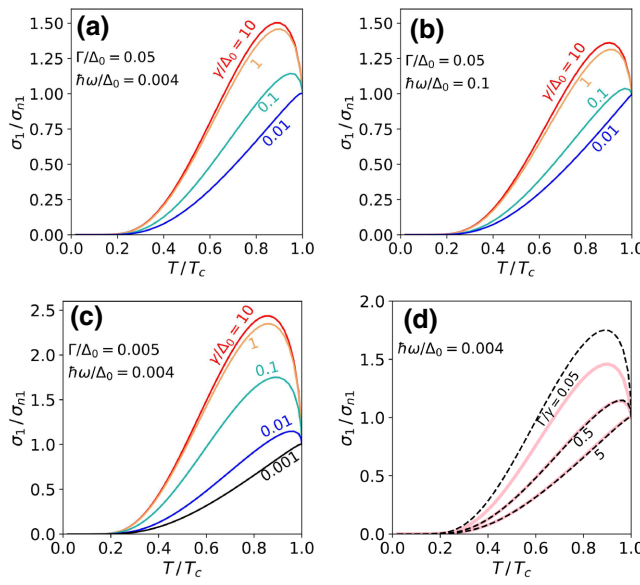


FIG. 5. Temperature dependence of  $\sigma_1(\gamma, \Gamma, T, \omega)$  for a  $T$ -independent constant  $\Gamma$ . (a)  $\Gamma/\Delta_0 = 0.05$  and  $\hbar\omega/\Delta_0 = 0.004$ . (b) A higher frequency:  $\hbar\omega/\Delta_0 = 0.1$ . (c) A smaller Dynes  $\Gamma$ :  $\Gamma/\Delta_0 = 0.005$ . The impurity concentration is varied from  $\gamma/\Delta_0 = 0.001$  (clean limit) to  $\gamma/\Delta_0 = 10$  (dirty limit). (d) Comparison between (a),(c). The solid-pink and dashed-black curves correspond to (a),(c), respectively. The solid and dashed curves for  $\Gamma/\gamma = 5$  and 0.5 almost overlap. See also the previous study [49] for the results of  $\omega \rightarrow 0$ .

Sec. IV B, we assume a  $T$ -independent constant  $\Gamma$  for simplicity, which would be a good starting point for investigating the temperature dependence of  $\sigma_1$ .

Shown in Fig. 5 are the temperature dependences of  $\sigma_1(\gamma, \Gamma, T, \omega)$  normalized by the real part of Drude's ac conductivity  $\sigma_{n1} = \sigma_n/[1 + (\omega\tau)^2]$ . Figure 5(a) is calculated for  $\Gamma/\Delta_0 = 0.05$ , the photon frequencies  $\hbar\omega/\Delta_0 = 0.004$ , and several different impurity concentrations. As the material gets clean (i.e., as  $\gamma/\Delta_0 = \pi\xi_0/2\ell_{\text{imp}}$  decreases), the height of the coherence peak decreases. This result might be counterintuitive, but it is consistent with the previous theoretical studies [49,94] and supported by experiments [96]. Figure 5(b) is calculated for the same  $\Gamma$  as (a) but a higher frequency ( $\hbar\omega/\Delta_0 = 0.1$ ) and shows that  $\omega$  reduces the height of the coherence peak. Figure 5(c) is calculated for the same frequency as (a) but for a smaller  $\Gamma$ , which shows  $\Gamma$  decreases the height of the coherence peak.

Shown in Fig. 5(d) is the comparison between (a) and (c). Interestingly, as first pointed out in Ref. [49], the temperature dependence of  $\sigma_1$  for a clean-limit superconductor does not depend on  $\Gamma$  and  $\gamma$  separately but on the ratio  $\Gamma/\gamma$  (see the curves for  $\Gamma/\gamma = 5$  and 0.5). Note that this is not the case for a dirty superconductor (see the curve for  $\Gamma/\gamma = 0.05$ ).

### C. Residual $\sigma_1$ at $T \rightarrow 0$

It is well known that  $\sigma_1$  of the idealized ( $\Gamma \rightarrow 0$ ) BCS superconductor vanishes at  $T \rightarrow 0$ . On the other hand, a realistic quasiparticle spectrum expressed with a finite  $\Gamma$  results in a residual  $\sigma_1$  at  $T \rightarrow 0$  due to finite subgap states at the Fermi level [2,3,21,43,49,53]. Suppose  $\hbar\omega/\Delta_0 \ll 1$ . Then, replacing  $\tanh(\epsilon/2k_B T)$  with the Heaviside step function and using  $g_{\pm} = \Gamma/\sqrt{\Gamma^2 + \Delta^2}$ ,  $f_{\pm} = \Delta/i\sqrt{\Gamma^2 + \Delta^2}$ , and  $d_{\pm} = i\sqrt{\Gamma^2 + \Delta^2} + i\gamma$ , Eq. (18) reduces to [49]

$$\sigma_1(\gamma, \Gamma, T, \omega)|_{T \rightarrow 0} = \sigma_n \frac{\gamma + \Gamma}{\gamma + \sqrt{\Gamma^2 + \Delta^2}} \frac{\Gamma^2}{\Gamma^2 + \Delta^2}. \quad (30)$$

Here,  $\Delta = \Delta(\Gamma, T)|_{T \rightarrow 0} = \Delta_0\sqrt{1 - 2\Gamma/\Delta_0}$  [see Eq. (7)]. In the dirty limit ( $\gamma/\Delta_0 = \pi\xi_0/2\ell_{\text{imp}} \gg 1$ ), we reproduce [3,21,22,43,53]

$$\sigma_1(\gamma, \Gamma, T, \omega)|_{T \rightarrow 0} = \sigma_n \frac{\Gamma^2}{\Gamma^2 + \Delta^2}. \quad (31)$$

Note that  $\sigma_n$  depends on electron relaxation time:  $\sigma_n \propto \tau$ .

Shown in Fig. 6(a) is the residual dissipative conductivity  $\lim_{T \rightarrow 0} \sigma_1$  as a function of the nonmagnetic impurity scattering rate  $\gamma$ . Note that  $\sigma_1$  is normalized by  $\sigma_0 = (2/3)e^2N_0v_f^2\tau_0 = (\tau_0/\tau)\sigma_n$ , independent of the electron mean free path in contrast to  $\sigma_n$ . Here,  $\tau_0$  is defined by  $\tau_0 = \hbar/2\Delta_0$ . The dashed-black curve is numerically calculated for  $\hbar\omega = 0.1$  and  $T/T_{c0} = 10^{-3}$ . The solid-green curve, calculated from Eq. (30), overlaps the dashed-black curve and is a good approximation as long as  $\hbar\omega \ll \Delta_0$ . We find the residual  $\sigma_1$  decreases as materials get dirty [see Eq. (31):  $\sigma_1 \propto \sigma_n \propto 1/\gamma$ ]. Shown in Fig. 6 (b) is  $\lim_{T \rightarrow 0} \sigma_1$  calculated for different  $\Gamma$  using Eq. (30). The residual  $\sigma_1$  increases as  $\Gamma$  increases (i.e., as subgap states at the Fermi level increase). Hence, the subgap-states-induced residual  $\sigma_1$  can be significantly suppressed by using a nearly ideal ( $\Gamma/\Delta_0 \ll 1$ ) dirty-limit ( $\gamma/\Delta_0 \gg 1$ ) superconductor.

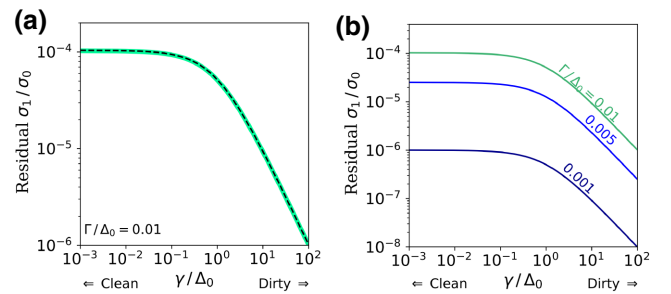


FIG. 6. (a) Residual  $\sigma_1$  at  $T \rightarrow 0$  as functions of the nonmagnetic impurity scattering rate  $\gamma/\Delta_0 = \pi\xi_0/2\ell_{\text{imp}}$  calculated for  $\Gamma/\Delta_0 = 0.01$ . The dashed-black curve is the numerical result for  $T/T_{c0} = 0.001$  and  $\hbar\omega/\Delta_0 = 0.1$ . The solid-green curve, which overlaps the dashed-black curve, is calculated from Eq. (30). (b) Residual  $\sigma_1$  at  $T \rightarrow 0$  as functions  $\gamma$  for different  $\Gamma$ .

#### D. Moderately low-temperature regime ( $\hbar\omega \ll k_B T \ll \Delta_0$ )

Type-II superconductors used for superconducting devices typically have the gap frequencies  $\Delta_0/2\pi\hbar \gtrsim$  several hundred GHz (e.g.,  $\Delta_0/2\pi\hbar \simeq 680$  GHz for Nb-Ti-N). Operating frequencies of devices are around 1–10 GHz and then satisfy  $\hbar\omega \ll \Delta_0$ . The operating temperature depends on the type of device, but almost all devices satisfy  $k_B T < 0.2k_B T_c \simeq 0.1\Delta_0 \ll \Delta_0$ . Hence, we may consider that a typical operating condition of superconducting microwave devices falls into the category of the low-frequency and low-temperature regime:  $\hbar\omega \ll \Delta_0$  and  $k_B T \ll \Delta_0$ . In particular, when  $\hbar\omega \ll k_B T \ll \Delta_0$ ,  $\sigma_1$  is mainly determined by thermally activated quasiparticles and is sensitive to the quasiparticle spectrum.

First, consider the idealized ( $\Gamma \rightarrow 0$ ) BCS superconductor in the dirty limit ( $\gamma/\Delta_0 = \pi\xi_0/2\ell_{\text{imp}} \gg 1$ ). When  $\hbar\omega \ll \Delta_0$  and  $k_B T \ll \Delta_0$ , the main contribution to the integral in Eq. (28) comes from a narrow strip of energy range  $0 < \bar{\epsilon} \lesssim k_B T (\ll \Delta)$ . Here, we define  $\bar{\epsilon} = \epsilon - \Delta$ . Then, the factor  $\epsilon^2 - \Delta^2$  reduces to  $\simeq 2\bar{\epsilon}\Delta$ , the distribution function reduces to  $f_{\text{FD}}(\epsilon) - f_{\text{FD}}(\epsilon + \hbar\omega) \simeq e^{-\Delta/k_B T} e^{-\bar{\epsilon}/k_B T} (1 - e^{-\hbar\omega/k_B T})$ , and then Eq. (28) results in the famous handy formula [3,5]:  $\sigma_1^{\text{dirty}}/\sigma_n = (4\Delta/\hbar\omega) e^{-\Delta/k_B T} \sinh(\hbar\omega/2k_B T) K_0(\hbar\omega/2k_B T)$ . Here, the modified Bessel function  $K_0(\hbar\omega/2k_B T)$  reduces to  $\simeq \ln(4k_B T/e^{\gamma_E}\hbar\omega)$  when  $\hbar\omega \ll k_B T$ . Hence, we find  $\sigma_1^{\text{dirty}} \propto \ln(1/\omega)$ . However, as materials get clean,  $\sigma_1$  exhibits a much different behavior from the dirty limit. Applying the similar calculation as above to Eq. (18), we find  $\sigma_1^{\text{clean}} \propto \omega^{-2}$  when  $\hbar\omega \ll k_B T \ll \Delta_0$ . Figure 7(a) shows  $\sigma_1$  of a nearly ideal ( $\Gamma/\Delta_0 = 0.001$ ) superconductor as functions of  $\omega$  for different impurity concentrations from the clean limit (black) to the dirty limit (red). A dirty-limit superconductor (red) exhibits  $\ln(1/\omega)$  dependence (see the red curve), while a clean-limit superconductor (black) exhibits  $\omega^{-2}$  dependence at  $\hbar\omega/\Delta \gtrsim 0.01$ . The black curve deviates from  $\omega^{-2}$  dependence at  $\hbar\omega \lesssim \gamma$ , where electrons can see the impurities during the rf period.

Finite subgap states can drastically change the  $\omega$  dependence of  $\sigma_1$ . Figure 7(b) is an example calculated for significantly smeared DOS peaks ( $\Gamma/\Delta_0 = 0.1$ , see also Fig. 1), in which  $\sigma_1$  is almost independent of  $\omega$ . Rather than such a large  $\Gamma$ , a relatively small  $\Gamma$  ( $\hbar\omega \lesssim \Gamma \ll k_B T \ll \Delta_0$ ) induces nontrivial effects. Figures 7(c) and 7(d) are  $\sigma_1$  for a clean and a dirty superconductor, respectively, calculated for different  $\Gamma$ . In both cases,  $\sigma_1$  for low-frequency regions ( $\hbar\omega \ll k_B T$ ) decreases as  $\Gamma$  increases, takes the minimum when  $\Gamma/\Delta_0 \sim 0.01$ –0.1, and then increases with  $\Gamma$ .

Figures 8(a) and 8(b) show  $\sigma_1$  as functions of Dynes  $\Gamma$ . In both the clean- and dirty-limit cases, the optimum value ( $\Gamma_*$ ) minimizes  $\sigma_1$ . In the clean (dirty) limit,  $\sigma_1(\Gamma_*)$  is  $\simeq 90\%$  (40%) smaller than that of the idealized ( $\Gamma \rightarrow 0$ )

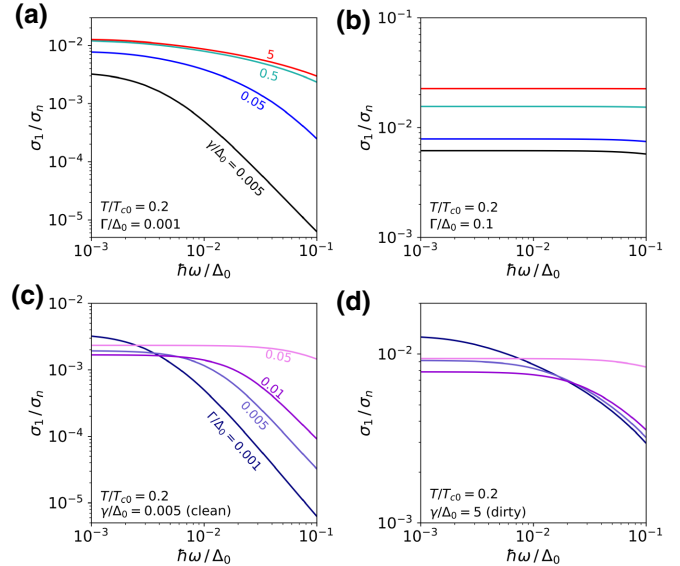


FIG. 7. The dissipative conductivity  $\sigma_1$  as functions of the photon frequency  $\omega$ . (a)  $\sigma_1$  of a nearly ideal ( $\Gamma/\Delta_0 = 0.001$ ) superconductor calculated for different nonmagnetic impurity scattering rate  $\gamma/\Delta_0 = \pi\xi_0/2\ell_{\text{imp}}$  from the clean limit to the dirty limit. (b)  $\sigma_1$  of a superconductor with strongly smeared gap peaks ( $\Gamma/\Delta_0 = 0.1$ ) calculated for different  $\gamma$ . (c)  $\sigma_1$  of a clean-limit ( $\gamma/\Delta_0 = 0.005$ ) superconductor calculated for different Dynes  $\Gamma$ . (d)  $\sigma_1$  of a dirty-limit ( $\gamma/\Delta_0 = 5$ ) superconductor calculated for different Dynes  $\Gamma$ .

BCS superconductor. These results can be qualitatively explained as follows. At moderately low temperatures,  $\hbar\omega \ll k_B T \ll \Delta_0$ ,  $\sigma_1$  is mainly determined by thermally activated quasiparticles and sensitive to the broadening of the DOS. For the dirty limit, the integral of the broadened quasiparticle spectrum with width approximately  $\Gamma > \hbar\omega$  yields  $\sigma \propto \log(1/\Gamma)$  [3,21,43,51]. As  $\Gamma$  increases,  $\sigma_1$  logarithmically decreases [see the slope at  $\Gamma \lesssim 0.01$  in Fig. 8(b)]. In the clean limit, in addition to the broadened quasiparticle spectrum, the  $d$  factor contributes to the integral, resulting in a sharper drop of  $\sigma_1 \propto \Gamma^{-1/2} \ln(1/\Gamma)$  [see the slope at  $\Gamma \lesssim 0.05$  in Fig. 8(a)].

According to Eq. (23), we have

$$\sigma_2(\gamma, \Gamma, T, \omega) = \frac{1}{\omega\mu_0\lambda^2(\gamma, \Gamma, T)}, \quad (32)$$

for  $\hbar\omega \ll \Delta_0$ . The same result can be derived from a simple discussion based on the local electrodynamics [3]. Suppose  $T \ll T_c$  and we have the quasistatic magnetic field  $B_z = B_0 e^{-x/\lambda} e^{-i\omega t}$  in a superconductor occupying  $x \geq 0$ . Then, Ampere's law and  $J_y = \sigma E_y \simeq i\sigma_2 E_y$  yield  $E_y = (B_0/\mu_0\sigma_2\lambda)e^{-\lambda/x}e^{-i(\omega t+\pi/2)}$ , while Faraday's law leads to the electric field  $E_y = \omega\lambda B_0 e^{-\lambda/x}e^{-i(\omega t+\pi/2)}$ . Then, we reproduce Eq. (32). Since the results are already shown in

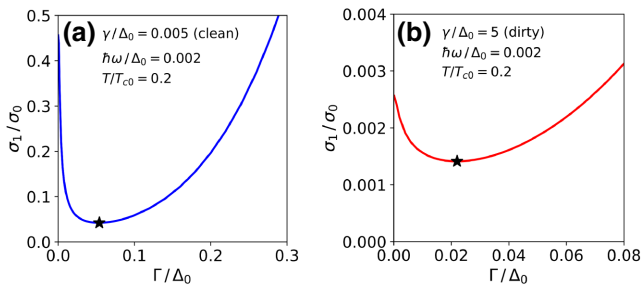


FIG. 8. The dissipative conductivity  $\sigma_1$  as functions of Dynes  $\Gamma$ . (a)  $\sigma_1$  of a clean-limit superconductor ( $\gamma/\Delta_0 = \pi\xi_0/2\ell_{\text{imp}} = 0.005$ ) and (b) a dirty-limit superconductor ( $\gamma/\Delta_0 = 5$ ). The stars represent the minimums.

Figs. 3 and 4, we do not repeat the calculations of  $\sigma_2$ . See Refs. [49,53,87] for calculations of  $\sigma_2$ .

### E. Quality factor and surface resistance

The electromagnetic response of a superconductor is generally nonlocal [17]. However, for an extreme type-II superconductor ( $\lambda \gg \xi$ ), a calculation reduces to a local problem, and the surface impedance  $Z_s$  is expressed with the complex conductivity. When  $\sigma_1/\sigma_2 \ll 1$  and the thickness of the material is larger than  $\lambda$ , we have

$$Z_s = R_s - iX_s = R_s + jX_s, \quad (33)$$

$$R_s = \frac{1}{2}\mu_0^2\omega^2\lambda^3\sigma_1, \quad (34)$$

$$X_s = \sqrt{\frac{\mu_0\omega}{\sigma_2}} = \mu_0\omega\lambda. \quad (35)$$

The quality factor  $Q = \omega U/P$  can be expressed with these quantities. Here,  $P = (1/2) \int R_s |\mathbf{H}|^2 dS$  and  $U = (\mu_0/2) \int |\mathbf{H}|^2 dV$  are the dissipation and the stored energy in the cavity, and  $dS$  and  $dV$  represent the area element and the volume element, respectively. Then, we have  $Q = \mu_0\omega \int |\mathbf{H}|^2 dV / \int R_s |\mathbf{H}|^2 dS$ , which simplifies to

$$Q = \frac{G}{R_s}, \quad (36)$$

$$G = \frac{\mu_0\omega \int |\mathbf{H}|^2 dV}{\int |\mathbf{H}|^2 dS}, \quad (37)$$

when  $R_s$  is uniform on the inner surface of the cavity. We can calculate  $R_s$  using the results of Secs. III–IV D and Eq. (34).

Shown in Fig. 9 (a) is  $R_s$  as functions of  $1/T$  for different impurity concentrations. Here, the normalization factor  $R_0$  is given by

$$R_0 = \frac{1}{2}\mu_0^2\tau_0^{-2}\lambda_0^3\sigma_0 = \frac{\mu_0\Delta_0\lambda_0}{\hbar}. \quad (38)$$

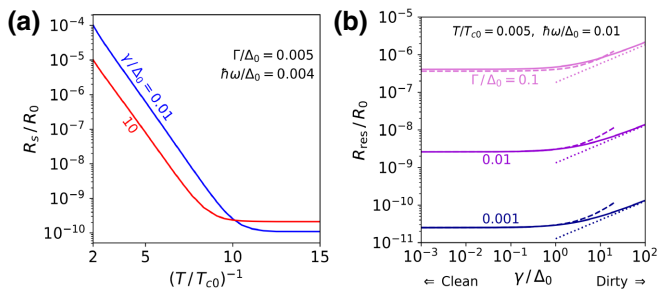


FIG. 9. (a) Surface resistance  $R_s$  as functions of  $1/T$ . Here, Dynes  $\Gamma$  is assumed independent of  $T$  for simplicity (see also Sec. IV B). (b) Subgap-state-induced residual surface resistance  $R_{\text{res}} = \lim_{T \rightarrow 0} R_s$  as functions of nonmagnetic impurity scattering rate  $\gamma/\Delta_0 = \pi\xi_0/2\ell_{\text{imp}}$  calculated for different Dynes  $\Gamma$ . The solid curves are numerically calculated for  $T/T_{c0} = 0.005$  and  $\hbar\omega/\Delta_0 = 0.01$ . The dashed and dotted curves are calculated from Eqs. (39) and (40), respectively.

For instances,  $R_0 \simeq 0.5\Omega$  and  $\simeq 0.8\Omega$  for  $\text{Nb}_3\text{Sn}$  and  $\text{Nb}-\text{Ti}-\text{N}$ , respectively. At higher temperatures, a dirty superconductor (red) exhibits smaller  $R_s$ . At lower temperatures, however,  $R_s$  of a clean superconductor (blue) becomes smaller than the red curve. Although the residual  $\sigma_1$  at  $T \rightarrow 0$  decreases as material gets dirtier (see Fig. 6), the contribution from  $\lambda^3$  significantly pushes up  $R_s$  of a dirty superconductor. Shown in Fig. 9(b) is the subgap-state-induced residual surface resistance  $R_{\text{res}} = \lim_{T \rightarrow 0} R_s$  as functions of the nonmagnetic impurity scattering rate  $\gamma/\Delta_0 = \pi\xi_0/2\ell_{\text{imp}}$  (solid curves).  $R_{\text{res}}$  is a monotonic increasing function of  $\gamma$  and  $\Gamma$ . For  $\Gamma/\Delta_0 \ll 1$  and  $\gamma/\Delta_0 \ll 1$  (clean limit), we find an analytical formula of  $R_{\text{res}}$  for a clean superconductor:

$$R_{\text{res}}^{\text{clean}} = \frac{R_0}{4} \left( \frac{\hbar\omega}{\Delta_0} \right)^2 \left( \frac{\Gamma}{\Delta_0} \right)^2 \left[ 1 + \frac{9\Gamma}{2\Delta_0} + \left( \frac{3\pi}{8} - 1 \right) \frac{\gamma}{\Delta_0} \right]. \quad (39)$$

Here, Eqs. (7), (12), and (30) are used. The dashed curves are calculated from Eq. (39), which agree well with the numerical results (solid curves) at  $\gamma/\Delta_0 \lesssim 1$ . For  $\Gamma/\Delta_0 \ll 1$  and  $\gamma/\Delta_0 \gg 1$  (dirty limit), using Eqs. (7), (14), and (31), we find

$$R_{\text{res}}^{\text{dirty}} = \frac{R_0}{\pi\sqrt{2\pi}} \left( \frac{\hbar\omega}{\Delta_0} \right)^2 \left( \frac{\Gamma}{\Delta_0} \right)^2 \sqrt{\frac{\gamma}{\Delta_0}} \left[ 1 + \left( \frac{7}{2} + \frac{3}{\pi} \right) \frac{\Gamma}{\Delta_0} \right]. \quad (40)$$

The dotted curves are calculated from Eq. (40) and agree with the numerical results (solid curves) at  $\gamma/\Delta_0 \gtrsim 10$ . Here, we focus on the subgap-state-induced  $R_{\text{res}}$ , which can be translated into the quality factor  $Q_\Gamma = G/R_{\text{res}}$ . Note that other factors [e.g., the two-level-system (TLS) defect [97], nonequilibrium quasiparticles [22,91], and trapped

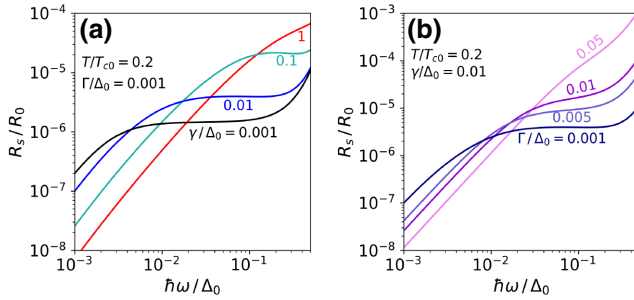


FIG. 10. Frequency dependences of the surface resistance  $R_s$ , (a) calculated for different nonmagnetic impurity scattering rate  $\gamma$  and (b) calculated for different Dynes  $\Gamma$ .

vortices [3]], can also contribute to the total  $Q$ :

$$Q^{-1} = Q_\Gamma^{-1} + Q_{\text{TLS}}^{-1} + \dots \quad (41)$$

Suppose  $\gamma/\Delta_0 \sim 1$ ,  $R_0 \sim 0.1\Omega$ , and  $G \sim 100\Omega$ . Then,  $\Gamma/\Delta_0 \sim 0.01$  and  $0.1$  yield  $Q_\Gamma^{-1} \sim 10^{-12}$  and  $10^{-10}$ , respectively. All other contributions need to be suppressed to a level below these values to observe  $Q_\Gamma^{-1}$ .

Next, consider  $R_s$  in the moderately-low-temperature regime ( $\hbar\omega \ll k_B T \ll \Delta_0$ ), which corresponds to an operating condition of some types of microwave resonators (e.g., SRF and KIDs). Figure 10(a) shows  $R_s$  of a nearly ideal BCS superconductor ( $\Gamma/\Delta_0 = 0.001 \ll 1$ ) as functions of  $\omega$  calculated for different impurity concentrations. The red curve corresponds to a dirty superconductor, exhibiting the famous  $\omega^2$  dependence well below the gap frequency (see, e.g., Ref. [98]). However, as the material gets clean (i.e., as  $\gamma$  decreases), a plateau appears. When  $\gamma/\Delta_0 = \pi\xi_0/2\ell_{\text{imp}} = 0.001$  (black curve),  $R_s$  is almost independent of  $\omega$  for a wide frequency range,  $0.005 \lesssim \hbar\omega/\Delta_0 \lesssim 0.1$ , corresponding to  $3.7 \text{ GHz} < f < 75 \text{ GHz}$  and  $3.4 \text{ GHz} < f < 68 \text{ GHz}$  for  $\text{Nb}_3\text{Sn}$  and  $\text{Nb}-\text{Ti}-\text{N}$ , respectively. This frequency-independent  $R_s$  comes from the  $\omega^{-2}$  dependence of  $\sigma_1$  in the clean limit (see Fig. 7) canceling out the  $\omega$  dependence of  $R_s \propto \omega^2\sigma_1$ , which occurs at  $\omega\tau \gtrsim 1$ . Shown in Fig. 10(b) is calculated for different Dynes  $\Gamma$ . As  $\Gamma$  increases, the plateau shrinks and disappears at  $\Gamma/\Delta_0 \sim 0.05$ . Only nearly ideal ( $\Gamma/\Delta_0 \ll 1$ ) clean-limit ( $\gamma/\Delta_0 \ll 1$ ) superconductors exhibit the plateau. It should be noted that this result is applicable to extreme type-II superconductors ( $\lambda \gg \xi$ ), while pure Al and pure Nb, which are popular resonator materials, do not fall into this category.

Now we investigate how to minimize  $R_s$  (i.e., maximize  $Q$ ). Shown in Fig. 11(a) is  $R_s$  as functions of nonmagnetic impurity scattering rate  $\gamma/\Delta_0 = \pi\xi_0/2\ell_{\text{imp}}$ . The navy curve is calculated for a nearly ideal BCS superconductor ( $\Gamma/\Delta_0 = 0.001$ ), whose minimum locates at  $\gamma/\Delta_0 \simeq 3$ , namely,  $\ell_{\text{imp}}/\xi_0 \simeq 0.5$ . The existence of the optimum mean-free path is very well known (see, e.g., Ref. [98]); its origin is the interplay of  $\lambda^3$  and  $\sigma_1$ , which

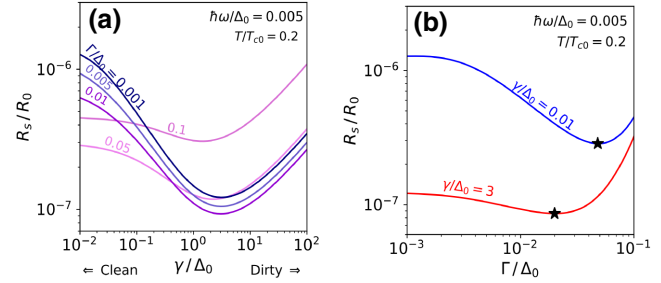


FIG. 11. (a)  $R_s$  as functions of nonmagnetic impurity scattering rate  $\gamma/\Delta_0 = \pi\xi_0/2\ell_{\text{imp}}$  calculated for different  $\Gamma$ . (b)  $R_s$  as functions of  $\Gamma$  calculated for  $\gamma/\Delta_0 = 3$  (red) and  $\gamma/\Delta_0 = 0.01$  (blue). The stars represent the minimums.

are increasing and decreasing functions of  $\gamma$ , respectively. As  $\Gamma$  increases, the minimum further decreases (see the dark-violet curve) and then increases at  $\Gamma/\Delta_0 \gtrsim 0.01$ . Figure 11(b) shows this nonmonotonic behavior as functions of  $\Gamma$ . The red curve is calculated for an optimally dirty superconductor ( $\gamma/\Delta_0 = 3$ ), reaching the minimum at  $\Gamma/\Delta_0 \simeq 0.02$ , where  $R_s$  is  $\simeq 30\%$  smaller than that of the ideal superconductor ( $\Gamma \rightarrow 0$ ) [21,22,43,51]. The blue curve is calculated for a clean superconductor ( $\gamma/\Delta_0 = 0.01$ ). Its minimum locates at  $\Gamma/\Delta_0 \simeq 0.05$ , where  $R_s$  is  $\simeq 80\%$  smaller than that of the ideal ( $\Gamma \rightarrow 0$ ) superconductor. The reduction of  $R_s$  due to a finite  $\Gamma$  comes from  $\sigma_1(\Gamma)$ , which is discussed in detail in Sec. IV D (see also Fig. 8).

As mentioned above, we find that  $R_s$  of a clean ( $\gamma/\Delta_0 \ll 1$ ) and nearly ideal ( $\Gamma/\Delta_0 \ll 1$ ) superconductor can be frequency independent for a wide frequency range (see Fig. 10). For instance, the condition  $\gamma/\Delta_0 = \Gamma/\Delta_0 = 0.001$  yields the plateau with  $R_s/R_0 \sim 1 \times 10^{-6}$ , which is one order of magnitude larger than the global minimum for  $\hbar\omega/\Delta_0 = 0.005$  [see the star on the red curve in Fig. 11(b)]. However,  $R_s$  of such a dirty superconductor increases in proportion to  $\omega^2$  and exceeds  $R_s/R_0 \sim 10^{-5}$  at  $\hbar\omega/\Delta_0 = 0.1$ , while  $R_s$  of a clean and nearly ideal superconductor remains  $R_s/R_0 \sim 10^{-6}$  even at  $\hbar\omega/\Delta_0 = 0.1$  (see Fig. 10). Moderately dirty ( $\ell_{\text{imp}} \sim \xi_0$ ) superconductors are widely believed to minimize  $R_s$ , while a nearly ideal clean superconductor ( $\gamma/\Delta_0 \simeq \Gamma/\Delta_0 \simeq 0.001$ ) can yield much smaller  $R_s$  for moderately-high-frequency regions ( $\hbar\omega \gtrsim 0.01$ ) for an extreme type-II superconductor.

## V. DEPAIRING CURRENT DENSITY

The depairing current density  $J_d$  is the maximum value of the supercurrent density. To obtain  $J_d$ , we need to solve Eq. (2) and calculate the current density. The solution for  $|q| > 0$  is given by [20]

$$g_m = \frac{a + i \cos \theta}{\sqrt{(a + i \cos \theta)^2 + b^2}}, \quad (42)$$

$$f_m = \frac{b}{\sqrt{(a + i \cos \theta)^2 + b^2}}. \quad (43)$$

Here  $a$ ,  $b$ ,  $\langle g_m \rangle$ , and  $\langle f_m \rangle$  are given by

$$\hbar\omega_m + \Gamma + \langle g_m \rangle \gamma - \frac{\pi s}{2} a = 0, \quad (44)$$

$$\Delta + \langle f_m \rangle \gamma - \frac{\pi s}{2} b = 0, \quad (45)$$

$$\langle g_m \rangle^4 + (a^2 + b^2 - 1) \langle g_m \rangle^2 - a^2 = 0, \quad (46)$$

$$\frac{\langle f_m \rangle}{b} = \tan^{-1} \frac{\langle g_m \rangle}{a}, \quad (47)$$

and  $\Delta = \Delta(s, \gamma, \Gamma, T)$  satisfies Eq. (4). The current density can be calculated from [16]  $\mathbf{J} = -4\pi k_B T e N_0 \text{Im} \sum_{\omega_m > 0} \langle \mathbf{v}_f g_m \rangle$

$$\frac{J}{J_0} = -\frac{\sqrt{6}\pi k_B T}{\Delta_0} \sum_{\omega_m > 0} \int_{-1}^1 dc \{ c \sin u(c) \sin v(c) \}. \quad (48)$$

Here,  $u + iv = \tan^{-1}[b/(a + ic)]$ ,  $c = \cos \theta$ ,  $J_0 = H_{c0}/\lambda_0$ ,  $H_{c0} = \Delta_0 \sqrt{N_0/\mu_0}$  is the thermodynamic critical field of the idealized BCS superconductor ( $\Gamma \rightarrow 0$ ) in the zero-current state, and  $\lambda_0 = \lambda(0, 0, 0)$  is the zero-temperature ( $T \rightarrow 0$ ) penetration depth of the idealized ( $\Gamma \rightarrow 0$ ) clean-limit ( $\gamma \rightarrow 0$ ) BCS superconductor in the zero-current state (see also Sec. III A).

Let us briefly review the depairing current density for the idealized ( $\Gamma \rightarrow 0$ ) BCS superconductor. Figure 12 shows the pair potential  $\Delta$  and the current density  $J$  as functions of the superfluid momentum  $q/q_0 = s/\Delta_0$  for the idealized BCS superconductor ( $\Gamma \rightarrow 0$ ) in the clean limit ( $\gamma \rightarrow 0$ ) calculated for different temperatures. When  $|q|$  is small, the current pair-breaking effect is limited [Fig. 12(a)], and  $J$  linearly increases with  $|q|$  [Fig. 12(b)]. However, as  $|q|$  increases, the reduction of  $\Delta$  becomes rapid [Fig. 12(a)], and  $J$  ceases to increase [Fig. 12(b)]. The maximum value of  $J$  (see the blob) is the depairing current density  $J_d(\gamma, \Gamma, T)$ . Interestingly, when  $T/T_{c0} \ll 1$ ,

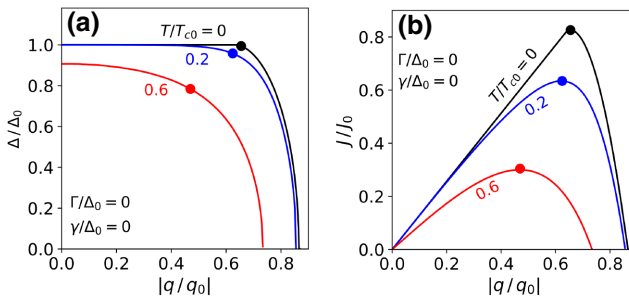


FIG. 12. (a)  $\Delta$  and (b)  $J$  for the idealized BCS superconductor ( $\Gamma \rightarrow 0$ ) in the clean limit ( $\gamma = 0$ ) calculated for  $T/T_{c0} = 0, 0.2$ , and  $0.6$ . The blobs correspond to the depairing current densities.

a finite  $|q|$  little affects  $\Delta$  up to a large momentum close to the depairing momentum. For  $\gamma = \Gamma = T = 0$  (i.e., the black curve), the solution is well known [15,19,20]. The pair potential  $\Delta = \Delta(s, 0, 0, 0)$  is given by

$$\ln \frac{\Delta}{\Delta_0} = \begin{cases} 0 & (s/\Delta \leq 2/\pi) \\ -\cosh^{-1} \frac{\pi s}{2\Delta} + \sqrt{1 - (2\Delta/\pi s)^2} & (s/\Delta > 2/\pi) \end{cases}, \quad (49)$$

and the current density  $J = J(s, 0, 0, 0)$  is given by

$$\frac{J}{J_0} = \frac{\pi s}{\sqrt{6}\Delta_0} \begin{cases} 1 & (s/\Delta \leq 2/\pi) \\ 1 - \{1 - (2\Delta/\pi s)^2\}^{3/2} & (s/\Delta > 2/\pi) \end{cases}, \quad (50)$$

which reaches the depairing current density,

$$J_d(0, 0, 0) = 0.826 \frac{H_{c0}}{\lambda_0}, \quad (51)$$

at the depairing momentum  $q_d/q_0 = s_d/\Delta_0 = 0.655$ . According to Eq. (49),  $\Delta$  is unaffected by the superfluid flow for  $q/q_0 = s/\Delta_0 \leq 0.637$ , which is very close to the depairing momentum. The nonexistence of current pair-breaking for a broad range of  $q$  is the well-known anomalous feature of a clean-limit superconductor at  $T/T_{c0} \ll 1$ . It should be noted that this feature disappears as  $T$  increases (see the red curve); also impure superconductors do not exhibit such an anomalous feature even at  $T \rightarrow 0$  (see the dirty-limit results [18,43,44,89] and Fig. 13). Shown in Fig. 13 are  $J(q)$  and  $\Delta(J)$  of the idealized BCS superconductor ( $\Gamma \rightarrow 0$ ) calculated for different impurity concentrations. As  $\gamma$  increases (as materials get dirty),  $J_d$  and  $\Delta(J)|_{J \sim J_d}$  decrease: nonmagnetic impurities

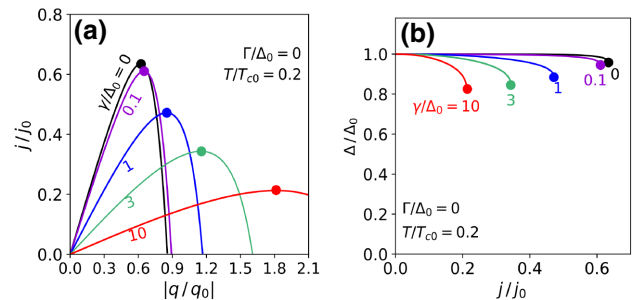


FIG. 13. Effects of impurity scattering rate  $\gamma$  (see also the previous studies [19,20]). (a)  $J$  as functions of  $q$  for the idealized BCS superconductor ( $\Gamma \rightarrow 0$ ) calculated for  $\gamma/\Delta_0 = \pi\xi_0/2\ell_{\text{imp}} = 0, 0.1, 1, 3$ , and  $10$ . (b)  $\Delta$  as functions of  $J$  calculated for  $J \leq J_d$ . The blobs represent the depairing current densities.

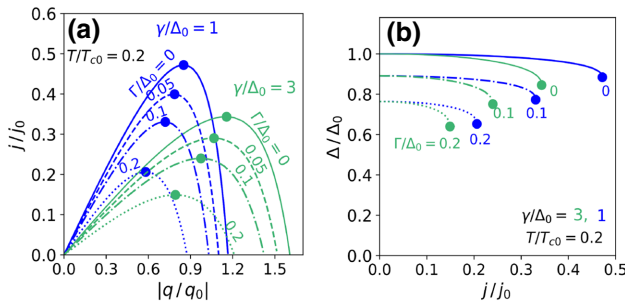


FIG. 14. Effects of Dynes  $\Gamma$  on  $J(q)$  and  $\Delta(J)$ . (a)  $J$  as functions of the superfluid momentum  $q$  calculated for  $\gamma/\Delta_0 = 1$  and 3 and  $\Gamma/\Delta_0 = 0, 0.05, 0.1$ , and 0.2. The blobs correspond to the depairing current densities. (b)  $\Delta$  as functions of  $J$  calculated for  $J \leq J_d$ .

become pair breakers and significantly impact  $\Delta$  in the current-carrying state, in contrast to their pair-conserving nature in the zero-current state (see Sec. II B).

Shown in Fig. 14 are the effects of Dynes  $\Gamma$  on  $J(q)$  and  $\Delta(J)$ . As  $\Gamma$  increases,  $J_d$  and  $\Delta$  decrease. In contrast to nonmagnetic impurities, Dynes  $\Gamma$  is always pair breaking even in the zero-current state as shown in Sec. II B; compare Fig. 13(b) with Fig. 14(b).

Figure 15(a) shows  $J_d$  as functions of the nonmagnetic impurity scattering rate  $\gamma/\Delta_0 = \pi\xi_0/2\ell_{\text{imp}}$ ;  $J_d$  decreases as  $\gamma$  increases (see also Fig. 13). At  $\gamma/\Delta_0 \gtrsim 1$ , we have  $J_d \propto \gamma^{-1/2}$ , consistent with the dirty-limit result [18,43,44,89]:

$$J_d(\gamma \gg \Delta_0, \Gamma, T) = C(\Gamma, T) \frac{H_{c0}}{\lambda_{0,\text{dirty}}} \propto \frac{1}{\sqrt{\gamma}}. \quad (52)$$

Here,  $\lambda_{0,\text{dirty}} = \sqrt{\hbar\rho_n/\pi\mu_0\Delta_0} \propto \sqrt{\gamma}$  is the zero-temperature penetration depth of the idealized ( $\Gamma \rightarrow 0$ ) dirty-limit BCS superconductor for the zero-current state (see also Sec. III A), and the coefficient  $C(\Gamma, T)$  can be calculated from the microscopic theory, e.g.,  $C(0, 0) = 0.595$  and  $C(0, T)$  are calculated some decades ago [18,19];  $C(\Gamma, T)$  is calculated in Refs. [43,44]. Figure 15(b) shows

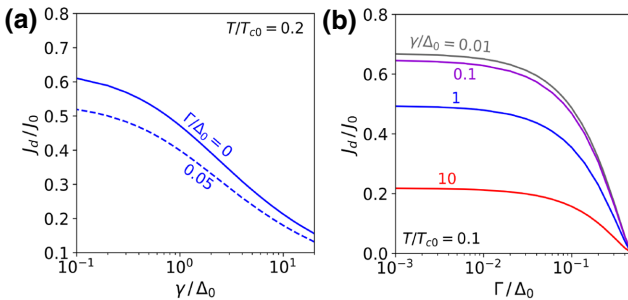


FIG. 15. The depairing current density  $J_d$  as functions of (a) the nonmagnetic impurity scattering rate  $\gamma/\Delta_0 = \pi\xi_0/2\ell_{\text{imp}}$  and (b) Dynes  $\Gamma$  parameter.

$J_d$  as functions of Dynes  $\Gamma$  for different impurity concentrations;  $J_d$  is significantly suppressed at  $\Gamma/\Delta_0 \gtrsim 0.1$ , where the pair-breaking scattering almost destroys the superconductivity.

## VI. DISCUSSION

The effects of Dynes  $\Gamma$  and nonmagnetic impurity scattering rate  $\gamma \propto \xi_0/\ell_{\text{imp}}$  on various physical quantities relevant to superconducting devices have been investigated. Here, we summarize our results and discuss their implications for superconducting devices.

### A. Kinetic inductance

In Sec. III, we calculate the penetration depth  $\lambda$  and the kinetic inductivity  $L_k$  taking the effects of  $\Gamma$  and  $\gamma$  into account and show that  $\lambda$  and  $L_k$  are monotonic increasing functions of  $\Gamma$  and  $\gamma$  (see Figs. 3 and 4). Equation (12) can evaluate  $\lambda$  for a nearly ideal ( $\Gamma/\Delta_0 \ll 1$ ) and clean ( $\gamma/\Delta_0 \ll 1$ ) BCS superconductor. Equations (13)–(15) give other convenient formulas for  $\lambda$ . Combining these formulas with Eqs. (16) and (17), we get the analytical formulas for  $L_k$ . Note that Eq. (15) is widely used for analyses of experimental data of superconducting devices, but it is applicable only to the idealized ( $\Gamma \rightarrow 0$ ) dirty-limit ( $\gamma/\Delta_0 = \pi\xi_0/\ell_{\text{imp}} \gg 1$ ) superconductor. To analyze a wide range of materials, Eqs. (12)–(17) or the numerical results (Figs. 3 and 4) would be helpful.

The reset time of SSPD is known to be limited by the kinetic inductance [54], and therefore nanowires with smaller kinetic inductances have been developed. On the other hand, a high kinetic inductance has also attracted attention in the quantum-circuit community; the so-called superinductor makes fluxonium qubit immune to charge fluctuations (see, e.g., Ref. [99]). According to our results, not only  $\gamma$  (impurity concentration) but also  $\Gamma$  increase  $L_k$ . The effect of  $\Gamma$  on  $L_k$  would not be negligible. However,  $\Gamma$  in the material of SSPDs, KIDs, and other quantum circuits is usually not measured. Measurements of  $\Gamma$  of circuit material using tunneling spectroscopy [23], AIPES [32], or recently proposed method to extract  $\Gamma$  from complex conductivity measurements [49,50], which will be discussed in Sec. VI B, would give insight into a method to engineer  $L_k$ .

### B. $T$ dependence of $\sigma_1$ and coherence peak

In Sec. IV B, we study the effects of  $\Gamma$  and  $\gamma$  on the  $T$  dependence of  $\sigma_1$  and the coherence peak. The height of the coherence peak decreases as  $\omega$  or  $\ell_{\text{imp}} (\propto \gamma^{-1})$  increases, consistent with the previous theoretical study [49,94] and experiment [96]. Note that the peak height decreases as the material gets clean. Also, a finite  $\Gamma$  reduces the peak height, consistent with the previous studies for the dirty-limit superconductor [43,53].

The recent finding of Ref. [49] was also reproduced: the  $\sigma_1(T)$  curve for a clean superconductor does not depend on  $\Gamma$  and  $\gamma$  separately but depends on the ratio  $\Gamma/\gamma$  [see Fig. 5(d)]. Also, it is possible to extract  $\Gamma$  and  $\gamma$  by fitting experimental data with the theory as proposed in Ref. [49], in which they evaluated  $\Gamma$  and  $\gamma$  using the recent experimental data of SRF resonant cavities [50]. This method would apply to KIDs and other resonators for quantum technologies. Now,  $\Gamma$  of resonator material can be easily obtained via measurements of  $\sigma_1$ , which are routinely performed in laboratories. Using experimentally determined  $\Gamma$ , it becomes possible to compare experimental data of devices with the more realistic theories [21,22,43,44] rather than the simplest formulas such as Eqs. (15) and (28).

### C. $\sigma_1$ and $R_s$ at a very low $T$

In Secs. IV C and IV E, we calculate the subgap-state-induced residual-dissipative-conductivity  $\lim_{T \rightarrow 0} \sigma_1$  and residual surface resistance  $R_{\text{res}} = \lim_{T \rightarrow 0} R_s$ , which originates from a finite density of subgap states in the vicinity of the Fermi level (see Figs. 6 and 9). Equations (30) and (31) are formulas for  $\lim_{T \rightarrow 0} \sigma_1$ . Also, we derive the formulas for  $R_{\text{res}}$ , Eqs. (39) and (40), which give good approximations of the numerical results of  $R_{\text{res}}$  [see Fig. 9(b)].

These results can be tested by experiments: measure the temperature dependence of  $\sigma_1$ , extract  $\Gamma$  and  $\gamma$  from  $\sigma_1(T)$  using Refs. [49,50], and cool a resonator down until  $Q$  becomes independent of  $T$ . However, as shown in Eq. (41), factors other than the subgap-state-induced  $R_{\text{res}}$  can also contribute to  $Q$ . Such contributions should be reduced to a level ignorable as compared with  $Q_{\Gamma}^{-1} = R_{\text{res}}/G$ , which is typically  $< 10^{-10}$  (see Sec. IV E). It would be difficult for a two-dimensional resonator to detect  $Q_{\Gamma}^{-1}$ , in which  $Q_{\text{TLS}}^{-1}$  always overwhelms  $Q_{\Gamma}^{-1}$ . High- $Q$  SRF cavities [61] may be helpful for this purpose.

### D. $\sigma_1$ and $R_s$ at a moderately low $T$

In Secs. IV D and IV E, we study  $\sigma_1$  and  $R_s$  at moderately low temperatures,  $\hbar\omega \ll k_B T \ll \Delta_0$ .

It is found that  $\sigma_1$  of a dirty superconductor exhibits the well-known frequency dependence  $\propto \ln(1/\omega)$ , while that of a nearly ideal ( $\Gamma/\Delta_0 \ll 1$ ) clean ( $\gamma/\Delta_0 = \pi\xi_0/2\ell_{\text{imp}} \ll 1$ ) superconductor exhibits  $\omega^{-2}$  dependence (see Fig. 7), resulting in the frequency-independent surface resistance  $R_s$ , shown in Fig. 10. For instance,  $R_s$  of a nearly ideal ( $\Gamma/\Delta_0 = 0.001$ ) clean-limit ( $\gamma/\Delta_0 = 0.001$ ) superconducting resonator made from a large- $\lambda/\xi$  material (e.g., Nb<sub>3</sub>Sn, Nb-Ti-N) is frequency independent between a few GHz and several tens of GHz (e.g., 3.7 GHz  $\lesssim f \lesssim$  75 GHz for Nb<sub>3</sub>Sn). Roughly speaking, the red curve in Fig. 10(a) corresponds to a dirty Nb<sub>3</sub>Sn cavity operated at  $T \sim 4$  K. When the resonant frequency is  $f \sim 1$  GHz,

which corresponds to  $\hbar\omega/\Delta_0 = 10^{-3}$ , its surface resistance is  $R_s \sim n\Omega$  from Fig. 10(a), consistent with experiments. The frequency-independent  $R_s$  is realized when the material is nearly ideal and clean (the black curve).  $R_s$  of the black curve is one order of magnitude larger than the red curve at  $\hbar\omega/\Delta_0 = 10^{-3}$  (approximately 1 GHz) but smaller than the red curve at  $\hbar\omega/\Delta_0 \gtrsim 10^{-2}$  (approximately 10 GHz), where  $R_s \sim \mu\Omega$ . The red curve increases in proportion to  $\omega^2$ , while the black curve remains  $R_s \sim \mu\Omega$  even at  $\hbar\omega/\Delta_0 \sim 0.1$  (approximately 100 GHz). Hence, if there is a demand for a compact cavity with the resonant frequency approximately a few tens GHz, it should be made from a nearly ideal ( $\Gamma/\Delta_0 \ll 1$ ) clean-limit ( $\gamma/\Delta_0 \ll 1$ ) type-II superconductor to minimize  $R_s$ .

Also, it is found that  $\sigma_1$  and  $R_s$  are nonmonotonic functions of  $\Gamma$ , and there exists the optimum value  $\Gamma_*$ , which minimizes  $\sigma_1$  and  $R_s$ . For the dirty limit,  $\sigma_1(\Gamma_*)$  and  $R_s(\Gamma_*)$  are a few tens of % smaller than those of the idealized dirty-limit BCS superconductor, consistent with the previous studies [21,22]. On the other hand, for the clean limit,  $\sigma_1(\Gamma_*)$  and  $R_s(\Gamma_*)$  are one order of magnitude smaller than those of the idealized clean-limit BCS superconductor (see Figs. 8 and 11). It has been well known that the optimum impurity scattering rate  $\gamma/\Delta_0 \sim \xi_0/\ell_{\text{imp}} \sim 1$  minimizes  $R_s$ . Such an  $R_s$  minimized by the optimum  $\gamma$  can be further reduced by the optimum  $\Gamma$  [see Fig. 11]. These results suggest that we can significantly reduce  $R_s$  by tuning  $\Gamma$ . According to the previous experiments, doping appropriate impurities [26,30,50] can reduce  $\Gamma$  of Nb. While the physics and materials mechanisms behind  $\Gamma$  are not well understood, comparison of experimentally determined  $\Gamma$  (e.g., using tunneling spectroscopy [23], AIPES [32], or complex conductivity measurement [49,50]) and various materials treatments [26,50] can give useful information on how to engineer  $\Gamma$ .

In the present study, we focus on the weak-field regime. However, to understand the physics of particle accelerator cavities operated under a strong microwave field close to  $H_c$ , we need to extend the present theory to the field-dependent nonlinear regime. Such an extension requires formulating the field-dependent nonlinear surface resistance  $R_s(H_0)$  based on the Keldysh technique of the nonequilibrium Green's function. It should be noted that Ref. [22] found the nonequilibrium effect is negligible for some practical parameter space by using the Keldysh technique of the nonequilibrium Green's function and calculated  $R_s(H_0)$  using the quasiparticle spectrum under the strong rf current and the Fermi-Dirac distribution function, while the calculation based on the nonequilibrium distribution function remains the future challenge.

### E. Depairing current density

In Sec. V, we study the depairing current density  $J_d$ . As shown in Fig. 15,  $J_d$  is a monotonically decreasing function

of  $\Gamma$  and  $\gamma \propto \ell_{\text{imp}}^{-1}$ . Hence, we need both  $\Gamma$  and  $\gamma$  to know  $J_d$  of the materials of devices or cables. As repeatedly mentioned above, tunneling spectroscopy can determine  $\Gamma$ , and the  $T$  dependence of  $\sigma_1$  [49,50] can determine  $\Gamma$  and  $\gamma$ . Combining these measurements of  $\Gamma$  and  $\gamma$  with those of  $J_d$ , such as Refs. [100,101], we can test the theory. Also, combining various materials treatments and the  $\Gamma$  measurement can give beneficial information on ameliorating  $J_d$ , which is practically extremely useful to examine the quality of superconducting cable and a thin film laminated on the inner surface of a superconducting heterostructure cavity.

## ACKNOWLEDGMENTS

I want to express my most profound appreciation to all the people who kindly support my two-year paternity leave from April 2021. This work is supported by Toray Science Foundation Grant No. 19-6004.

## APPENDIX: CALCULATION CODES

The codes to calculate the physical quantities evaluated in the present paper are available from the author upon reasonable request.

- [1] H. Padamsee, 50 years of success for SRF accelerators—A review, *Supercond. Sci. Technol.* **30**, 053003 (2017).
- [2] A. Gurevich, Superconducting radio-frequency fundamentals for particle accelerators, *Rev. Accel. Sci. Technol.* **5**, 119 (2012).
- [3] A. Gurevich, Theory of RF superconductivity for resonant cavities, *Supercond. Sci. Technol.* **30**, 034004 (2017).
- [4] S. Eley, A. Glatz, and R. Willa, Challenges and transformative opportunities in superconductor vortex physics, *J. Appl. Phys.* **130**, 050901 (2021).
- [5] J. Zmuidzinas, Superconducting microresonators: Physics and applications, *Annu. Rev. Condens. Matter Phys.* **3**, 169 (2012).
- [6] T. M. Klapwijk and A. V. Semenov, Engineering physics of superconducting hot-electron bolometer mixers, *IEEE Trans. Terahertz Sci. Technol.* **7**, 627 (2017).
- [7] J. Zmuidzinas and P. L. Richards, Superconducting detectors and mixers for millimeter and submillimeter astrophysics, *Proc. IEEE* **92**, 1597 (2004).
- [8] C. M. Natarajan, M. G. Tanner, and R. H. Hadfield, Superconducting nanowire single-photon detectors: Physics and applications, *Supercond. Sci. Technol.* **25**, 063001 (2012).
- [9] A. Engel, J. J. Renema, K. Il'in, and A. Semenov, Detection mechanism of superconducting nanowire single-photon detectors, *Supercond. Sci. Technol.* **28**, 114003 (2015).
- [10] G. Wendin, Quantum information processing with superconducting circuits: A review, *Rep. Prog. Phys.* **80**, 106001 (2017).
- [11] E. Grumblig and M. Horowitz, *Quantum Computing: Progress and Prospects* (The National Academy Press, Washington, DC, 2019).
- [12] M. Tinkham, *Introduction to Superconductivity: Second Edition* (Dover Publications, New York, 2004).
- [13] P. G. De Gennes, *Superconductivity of Metals and Alloys* (Westview Press, Colorado, 1999).
- [14] A. A. Abrikosov, *Fundamentals of the Theory of Metals* (Elsevier, North-Holland, 1988).
- [15] K. Maki, in *Superconductivity*, edited by R. D. Parks (Marcel Dekker, Inc., New York, 1969), Vol. 2, p. 1035.
- [16] N. B. Kopnin, *Theory of Nonequilibrium Superconductivity* (Oxford University Press, Oxford, 2001).
- [17] D. C. Mattis and J. Bardeen, Theory of the anomalous skin effect in normal and superconducting metals, *Phys. Rev.* **111**, 412 (1958).
- [18] K. Maki, On persistent currents in a superconducting alloy I, *Prog. Theor. Phys.* **29**, 10 (1963).
- [19] M. Yu Kupriyanov and V. F. Lukichev, Temperature dependence of pair-breaking current in superconductors, *Fiz. Nizk. Temp.* **6**, 445 (1980).
- [20] F. Pei-Jen and A. Gurevich, Effect of impurities on the superheating field of type-II superconductors, *Phys. Rev. B* **85**, 054513 (2012).
- [21] A. Gurevich and T. Kubo, Surface impedance and optimum surface resistance of a superconductor with an imperfect surface, *Phys. Rev. B* **96**, 184515 (2017).
- [22] T. Kubo and A. Gurevich, Field-dependent nonlinear surface resistance and its optimization by surface nanstructuring in superconductors, *Phys. Rev. B* **100**, 064522 (2019).
- [23] J. Zasadzinski, in *The Physics of Superconductors*, edited by K. H. Bennemann and J. B. Ketterson (Springer, Berlin, 2003), Vol. 1, p. 591.
- [24] A. Kamlapure, M. Mondal, M. Chand, A. Mishra, J. Jesudasan, V. Bagwe, L. Benfatto, V. Tripathi, and P. Raychaudhuri, Measurement of magnetic penetration depth and superconducting energy gap in very thin epitaxial NbN films, *Appl. Phys. Lett.* **96**, 072509 (2010).
- [25] Y. Noat, V. Cherkez, C. Brun, T. Cren, C. Carbillot, F. Debontridder, K. Ilin, M. Siegel, A. Semenov, H.-W. Hubers, *et al.*, Unconventional superconductivity in ultrathin superconducting NbN films studied by scanning tunneling spectroscopy, *Phys. Rev. B* **88**, 014503, 2013.
- [26] P. Dhakal, G. Ciovati, G. R. Myneni, K. E. Gray, N. Groll, P. Maheshwari, D. M. McRae, R. Pike, T. Proslie, F. Stevie, *et al.*, Effect of high temperature heat treatments on the quality factor of a large-grain superconducting radiofrequency niobium cavity, *Phys. Rev. ST Accel. Beams* **16**, 042001 (2013).
- [27] N. R. Groll, J. A. Klug, C. Cao, S. Altin, H. Claus, N. G. Becker, J. F. Zasadzinski, M. J. Pellin, and T. Proslie, Tunneling spectroscopy of superconducting MoN and NbTiN grown by atomic layer deposition, *Appl. Phys. Lett.* **104**, 092602 (2014).
- [28] C. Becker, S. Posen, N. Groll, R. Cook, C. M. Schleputz, D. L. Hall, M. Liepe, M. Pellin, J. Zasadzinski, and T. Proslie, Analysis of Nb<sub>3</sub>Sn surface layers for superconducting radio frequency cavity applications, *Appl. Phys. Lett.* **106**, 082602 (2015).

- [29] P. Szabó, T. Samuely, V. Hašková, J. Kačmarčík, M. Žemlička, M. Grajcar, J. G. Rodrigo, and P. Samuely, Fermionic scenario for the destruction of superconductivity in ultrathin MoC films evidenced by STM measurements, *Phys. Rev. B* **93**, 014505 (2016).
- [30] E. M. Lechner, B. D. Oli, J. Makita, G. Ciovati, A. Gurevich, and M. Iavarone, Electron Tunneling and X-Ray Photoelectron Spectroscopy Studies of the Superconducting Properties of Nitrogen-Doped Niobium Resonator Cavities, *Phys. Rev. Appl.* **13**, 044044 (2020).
- [31] H. Boschker, E. Fillis-Tsirakis, C. Richter, D. Zhang, J. Smet, and L. Kuerten, Microscopic origin of the Dynes parameter  $\Gamma$  of the  $\text{LaAlO}_3 - \text{SrTiO}_3$  interface superconductor, *Phys. Rev. B* **102**, 134506 (2020).
- [32] T. Shimojima, K. Okazaki, and S. Shin, Low-temperature and high-energy-resolution laser photoemission spectroscopy, *J. Phys. Soc. Jpn.* **84**, 072001 (2015).
- [33] A. Chainani, T. Yokoya, T. Kiss, and S. Shin, Photoemission Spectroscopy of the Strong-Coupling Superconducting Transitions in Lead and Niobium, *Phys. Rev. Lett.* **85**, 1966 (2000).
- [34] S. B. Kaplan, C. C. Chi, D. N. Langenberg, J. J. Chang, S. Jafarey, and D. J. Scalapino, Quasiparticle and phonon lifetimes in superconductors, *Phys. Rev. B* **14**, 4854 (1976).
- [35] T. P. Devereaux and D. Belitz, Quasiparticle inelastic lifetimes in disordered superconducting films, *Phys. Rev. B* **44**, 4587 (1991).
- [36] D. A. Browne, K. Levin, and K. A. Muttalib, Coulomb-Induced Anomalies in Highly Disordered Superconductors: Application to Tunneling, *Phys. Rev. Lett.* **58**, 156 (1987).
- [37] A. J. Bennett, Theory of the anisotropic energy gap in superconducting lead, *Phys. Rev.* **140**, A1902 (1965).
- [38] A. I. Larkin and Y. N. Ovchinnikov, Density of states in inhomogeneous superconductors, *Sov. Phys. JETP* **34**, 1144 (1972).
- [39] A. V. Balatsky, I. Vekhter, and J.-X. Zhu, Impurity-induced states in conventional and unconventional superconductors, *Rev. Mod. Phys.* **78**, 373 (2006).
- [40] J. S. Meyer and B. D. Simons, Gap fluctuations in inhomogeneous superconductors, *Phys. Rev. B* **64**, 134516 (2001).
- [41] R. C. Dynes, V. Narayanamurti, and J. P. Garno, Direct Measurement of Quasiparticle-Lifetime Broadening in a Strong-Coupled Superconductor, *Phys. Rev. Lett.* **41**, 1509 (1978).
- [42] R. C. Dynes, J. P. Garno, G. B. Hertel, and T. P. Orlando, Tunneling Study of Superconductivity Near the Metal-Insulator Transition, *Phys. Rev. Lett.* **53**, 2437 (1984).
- [43] T. Kubo, Weak-field dissipative conductivity of a dirty superconductor with Dynes subgap states under a dc bias current up to the depairing current density, *Phys. Rev. Res.* **2**, 013302 (2020).
- [44] T. Kubo, Superfluid flow in disordered superconductors with Dynes pair-breaking scattering: Depairing current, kinetic inductance, and superheating field, *Phys. Rev. Res.* **2**, 033203 (2020).
- [45] F. Vischi, M. Carrega, E. Strambini, S. D'Ambrosio, F. S. Bergeret, Y. V. Nazarov, and F. Giazotto, Coherent transport properties of a three-terminal hybrid superconducting interferometer, *Phys. Rev. B* **95**, 054504 (2017).
- [46] G. Tang, W. Belzig, U. Zulicke, and C. Bruder, Signatures of the Higgs mode in transport through a normal-metal-superconductor junction, *Phys. Rev. Res.* **2**, 022068(R) (2020).
- [47] A. A. Mikhailovsky, S. V. Shulga, A. E. Karakozov, O. V. Dolgov, and E. G. Maksimov, Thermal pair-breaking in superconductors with strong electron-phonon interaction, *Solid State Commun.* **80**, 511 (1991).
- [48] F. Herman and R. Hlubina, Microscopic interpretation of the Dynes formula for the tunneling density of states, *Phys. Rev. B* **94**, 144508 (2016).
- [49] F. Herman and R. Hlubina, Microwave response of superconductors that obey local electrodynamics, *Phys. Rev. B* **104**, 094519 (2021).
- [50] D. Bafia, A. Grassellino, M. Checchin, J. F. Zasadzinski, and A. Romanenko, The anomalous resonant frequency variation of microwave superconducting niobium cavities near  $T_c$ , *ArXiv:2103.10601*.
- [51] A. Gurevich, Reduction of Dissipative Nonlinear Conductivity of Superconductors by Static and Microwave Magnetic Fields, *Phys. Rev. Lett.* **113**, 087001 (2014).
- [52] G. Ciovati, P. Dhakal, and A. Gurevich, Decrease of the surface resistance in superconducting niobium resonator cavities by the microwave field, *Appl. Phys. Lett.* **104**, 092601 (2014).
- [53] F. Herman and R. Hlubina, Electromagnetic properties of impure superconductors with pair-breaking processes, *Phys. Rev. B* **96**, 014509 (2017).
- [54] A. J. Kerman, E. A. Dauler, W. E. Keicher, J. K. W. Yang, K. K. Berggren, G. Gol'tsman, and B. Voronov, Kinetic-inductance-limited reset time of superconducting nanowire photon counters, *Appl. Phys. Lett.* **88**, 111116 (2006).
- [55] A. Romanenko, A. Grassellino, A. C. Crawford, D. A. Sergatskov, and O. Melnychuk, Ultra-high quality factors in superconducting niobium cavities in ambient magnetic fields up to 190 mG, *Appl. Phys. Lett.* **105**, 234103 (2014).
- [56] S. Huang, T. Kubo, and R. L. Geng, Dependence of trapped-flux-induced surface resistance of a large-grain Nb superconducting radio-frequency cavity on spatial temperature gradient during cooldown through  $T_c$ , *Phys. Rev. Accel. Beams* **19**, 082001 (2016).
- [57] S. Posen, M. Checchin, A. C. Crawford, A. Grassellino, M. Martinello, O. S. Melnychuk, A. Romanenko, D. A. Sergatskov, and Y. Trenikhina, Efficient expulsion of magnetic flux in superconducting radio frequency cavities for high  $Q_0$  applications, *J. Appl. Phys.* **119**, 213903 (2016).
- [58] M. Checchin, M. Martinello, A. Romanenko, A. Grassellino, D. A. Sergatskov, S. Posen, O. Melnychuk, and J. F. Zasadzinski, Quench-Induced Degradation of the Quality Factor in Superconducting Resonators, *Phys. Rev. Appl.* **5**, 044019 (2016).
- [59] S. Ooi, M. Tachiki, T. Konomi, T. Kubo, A. Kikuchi, S. Arisawa, H. Ito, and K. Umemori, Observation of intermediate mixed state in high-purity cavity-grade Nb by magneto-optical imaging, *Phys. Rev. B* **104**, 064504 (2021).

- [60] D. Longuevergne and A. Miyazaki, Impact of geometry on the magnetic flux trapping of superconducting accelerating cavities, *Phys. Rev. Accel. Beams* **24**, 083101 (2021).
- [61] A. Romanenko, R. Pilipenko, S. Zorzetti, D. Frolov, M. Awida, S. Belomestnykh, S. Posen, and A. Grassellino, Three-Dimensional Superconducting Resonators at  $T < 20$  mK with Photon Lifetimes up to  $\tau = 2$  s, *Phys. Rev. Appl.* **13**, 034032 (2020).
- [62] S. Posen, A. Romanenko, A. Grassellino, O. S. Melnychuk, and D. A. Sergatskov, Ultralow Surface Resistance Via Vacuum Heat Treatment of Superconducting Radio-Frequency Cavities, *Phys. Rev. Appl.* **13**, 014024 (2020).
- [63] H. Ito, H. Araki, K. Takahashi, and K. Umemori, Influence of furnace baking on Q-E behavior of superconducting accelerating cavities, *Prog. Theor. Exp. Phys.* **2021**, 071G01 (2021).
- [64] F. He, W. Pan, P. Sha, J. Zhai, Z. Mi, X. Dai, S. Jin, Z. Zhang, C. Dong, B. Liu, *et al.*, Medium-temperature furnace baking of 1.3 GHz 9-cell superconducting cavities at IHEP, *Supercond. Sci. Technol.* **34**, 095005 (2021).
- [65] R. L. Geng, G. V. Eremeev, H. Padamsee, and V. D. Shemelin, in *Proceedings of PAC07, Albuquerque, New Mexico, USA* (JACoW, CERN, Geneva, 2007), p. 2337.
- [66] T. Kubo, Y. Ajima, H. Inoue, K. Umemori, Y. Watanabe, and M. Yamanaka, in *Proceedings of IPAC2014, Dresden, Germany* (JACoW, CERN, Geneva, 2014), p. 2519...
- [67] A. Grassellino, A. Romanenko, Y. Trenikhina, M. Checchin, M. Martinello, O. S. Melnychuk, S. Chandrasekaran, D. A. Sergatskov, S. Posen, A. C. Crawford, *et al.*, Unprecedented quality factors at accelerating gradients up to  $45 \text{ MVm}^{-1}$  in niobium superconducting resonators via low temperature nitrogen infusion, *Supercond. Sci. Technol.* **30**, 094004 (2017).
- [68] P. Dhakal, S. Chetri, S. Balachandran, P. J. Lee, and G. Ciovati, Effect of low temperature baking in nitrogen on the performance of a niobium superconducting radio frequency cavity, *Phys. Rev. Accel. Beams* **21**, 032001 (2018).
- [69] A. Gurevich, Enhancement of rf breakdown field of superconductors by multilayer coating, *Appl. Phys. Lett.* **88**, 012511 (2006).
- [70] T. Kubo, Y. Iwashita, and T. Saeki, Radio-frequency electromagnetic field and vortex penetration in multilayered superconductors, *Appl. Phys. Lett.* **104**, 032603 (2014).
- [71] A. Gurevich, Maximum screening fields of superconducting multilayer structures, *AIP Adv.* **5**, 017112 (2015).
- [72] D. B. Liarte, S. Posen, M. K. Transtrum, G. Catelani, M. Liepe, and J. P. Sethna, Theoretical estimates of maximum fields in superconducting resonant radio frequency cavities: Stability theory, disorder, and laminates, *Supercond. Sci. Technol.* **30**, 033002 (2017).
- [73] T. Kubo, Multilayer coating for higher accelerating fields in superconducting radio-frequency cavities: A review of theoretical aspects, *Supercond. Sci. Technol.* **30**, 023001 (2017).
- [74] T. Kubo, Superheating fields of semi-infinite superconductors and layered superconductors in the diffusive limit: Structural optimization based on the microscopic theory, *Supercond. Sci. Technol.* **34**, 045006 (2021).
- [75] A-M. Valente-Feliciano, Superconducting RF materials other than bulk niobium: A review, *Supercond. Sci. Technol.* **29**, 113002 (2016).
- [76] S. Posen and D. L. Hall, Nb<sub>3</sub>Sn superconducting radiofrequency cavities: Fabrication, results, properties, and prospects, *Supercond. Sci. Technol.* **30**, 033004 (2017).
- [77] T. Tan, M. A. Wolak, X. X. Xi, T. Tajima, and L. Civale, Magnesium diboride coated bulk niobium: A new approach to higher acceleration gradient, *Sci. Rep.* **6**, 35879 (2016).
- [78] T. Junginger, S. H. Abidi, R. D. Maffett, T. Buck, M. H. Dehn, S. Gheidi, R. Kiefl, P. Kolb, D. Storey, E. Thoeng, *et al.*, Field of first magnetic flux entry and pinning strength of superconductors for rf application measured with muon spin rotation, *Phys. Rev. Accel. Beams* **21**, 032002 (2018).
- [79] C. Z. Antoine, M. Aburas, A. Four, F. Weiss, Y. Iwashita, H. Hayano, S. Kato, T. Kubo, and T. Saeki, Optimization of tailored multilayer superconductors for RF application and protection against premature vortex penetration, *Supercond. Sci. Technol.* **32**, 085005 (2019).
- [80] S. Keckert, T. Junginger, T. Buck, D. Hall, P. Kolb, O. Kugeler, R. Laxdal, M. Liepe, S. Posen, T. Prokscha, *et al.*, Critical fields of Nb<sub>3</sub>Sn prepared for superconducting cavities, *Supercond. Sci. Technol.* **32**, 075004 (2019).
- [81] E. Thoeng, T. Junginger, P. Kolb, B. Matheson, G. Morris, N. Muller, S. Saminathan, R. Baartman, and R. E. Laxdal, in *Proceedings of SRF2019, Dresden, Germany* (JACoW, CERN, Geneva, 2019), p. 966.
- [82] H. Ito, H. Hayano, T. Kubo, and T. Saeki, Vortex penetration field measurement system based on third-harmonic method for superconducting RF materials, *Nucl. Instrum. Methods Phys. Res. A* **955**, 163284 (2020).
- [83] Z. Lin, M. Qin, D. Li, P. Shen, L. Zhang, Z. Feng, P. Sha, J. Miao, J. Yuan, X. Dong, *et al.*, Enhancement of the lower critical field in FeSe-coated Nb structures for superconducting radio-frequency applications, *Supercond. Sci. Technol.* **34**, 015001 (2021).
- [84] S. Leith, M. Vogel, J. Fan, E. Seiler, R. Ries, and X. Jiang, Superconducting NbN thin films for use in superconducting radio frequency cavities, *Supercond. Sci. Technol.* **34**, 025006 (2021).
- [85] I. H. Senevirathne, A. Gurevich, J. R. Delayen, and A.-M. Valente-Feliciano, in *Proceedings of IPA2021, Campinas, SP, Brazil* (JACoW, CERN, Geneva, 2021), p. 1208.
- [86] G. Eilenberger, Transformation of Gorkov's equation for type II superconductors into transport-like equations, *Z. Phys.* **214**, 195 (1968).
- [87] F. Marsiglio and J. P. Carbotte, in *The Physics of Superconductors*, edited by K. H. Bennemann and J. B. Ketterson (Springer, Berlin, 2003), Vol. 1, p. 73.
- [88] A. J. Annunziata, D. F. Santavicca, L. Frunzio, G. Catelani, M. J. Rooks, A. Frydman, and D. E. Prober, Tunable superconducting nanoinductors, *Nanotechnology* **21**, 445202 (2010).
- [89] J. R. Clem and V. G. Kogan, Kinetic impedance and depairing in thin and narrow superconducting films, *Phys. Rev. B* **86**, 174521 (2012).

- [90] A. V. Semenov, I. A. Devyatov, P. J. de Visser, and T. M. Klapwijk, Coherent Excited States in Superconductors due to a Microwave Field, *Phys. Rev. Lett.* **117**, 047002 (2016).
- [91] P. J. de Visser, D. J. Goldie, P. Diener, S. Withington, J. J. A. Baselmans, and T. M. Klapwijk, Evidence of a Nonequilibrium Distribution of Quasiparticles in the Microwave Response of a Superconducting Aluminum Resonator, *Phys. Rev. Lett.* **112**, 047004 (2014).
- [92] S. B. Nam, Theory of electromagnetic properties of superconducting and normal systems. I, *Phys. Rev.* **156**, 470 (1967).
- [93] W. Zimmermann, E. Brandt, M. Bauer, E. Seider, and L. Genzel, Optical conductivity of BCS superconductors with arbitrary purity, *Physica C* **183**, 99 (1991).
- [94] F. Marsiglio, Coherence effects in electromagnetic absorption in superconductors, *Phys. Rev. B* **44**, 5373 (1991).
- [95] D. Rainer and J. A. Sauls, in *Superconductivity: From Basic Physics to the Latest Developments*, edited by P. N. Butcher and Y. Lu (World Scientific, Singapore, 1995), p. 45.
- [96] K. Steinberg, M. Scheffler, and M. Dressel, Quasiparticle response of superconducting aluminum to electromagnetic radiation, *Phys. Rev. B* **77**, 214517 (2008).
- [97] C. Müller, J. H. Cole, and J. Lisenfeld, Towards understanding two-level-systems in amorphous solids: Insights from quantum circuits, *Rep. Prog. Phys.* **82**, 124501 (2019).
- [98] J. P. Turneaure, J. Halbritter, and H. A. Schwettman, The surface impedance of superconductors and normal conductors: The Mattis-Bardeen theory, *J. Supercond.* **4**, 341 (1991).
- [99] D. Niepce, J. Burnett, and J. Bylander, High Kinetic Inductance NbN Nanowire Superinductors, *Phys. Rev. Appl.* **11**, 044014 (2019).
- [100] J. Romijn, T. M. Klapwijk, M. J. Renne, and J. E. Mooij, Critical pair-breaking current in superconducting aluminum strips far below  $T_c$ , *Phys. Rev. B* **26**, 3648 (1982).
- [101] A. Y. Rusanov, M. B. S. Hesselberth, and J. Aarts, Depairing currents in superconducting films of Nb and amorphous MoGe, *Phys. Rev. B* **70**, 024510 (2004).